# Permian metabasalt and Triassic alkaline dykes in the northern Ivrea zone : clues to the post-Variscan geodynamic evolution of the Southern Alps

Autor(en): **Stähle, Volker / Frenzel, Gerhard / Hess, Jürgen C.**

Objekttyp: **Article**

Zeitschrift: **Schweizerische mineralogische und petrographische Mitteilungen = Bulletin suisse de minéralogie et pétrographie**

Band (Jahr): **81 (2001)**

Heft 1

PDF erstellt am: **11.07.2024**

Persistenter Link: https://doi.org/10.5169/seals-61677

SCHWEIZ. MINERAL. PETROGR. MITT. 81, 1–21, 2001

# Permian metabasalt and Triassic alkaline dykes in the northern Ivrea zone: clues to the post-Variscan geodynamic evolution of the Southern Alps

by *Volker Stähle*[1], *Gerhard Frenzel*[1], *Jürgen C. Hess*[2], *François Saupé*[3], *Susanne Th. Schmidt*[4] and *Werner Schneider*[5]

**Abstract**

The voluminous Lower Permian metabasalts/metagabbros ("Mafic Formation") in the northern Ivrea zone belong geodynamically to the post-Variscan calc-alkaline magmatism of Central Europe. East of Finero, the mafic magmatic rocks have low mean mg#-values of 51.9 and their distinctive Ni and Cr depletion indicates highly fractionated tholeiitic rocks. The fractionated state of the basaltic rocks requires that huge masses of olivine/clinopyroxene parental rocks exist, probably at the former crust/mantle boundary. These dense cumulitic rocks at shallow crustal-level may be responsible for the observed gravity anomaly along the Ivrea zone in the Western Alps.

The alkaline zircon syenite pegmatites, hornblende syenites and a carbonate-bearing hornblendite in the studied area are part of the Triassic magmatism in the Southern Alps. These pegmatitic dyke rocks may represent early signs of the metasomatism in the lithosphere as a prelude to the "Tethyan cycle". The magmas originated from partial melting of metasomatized upper mantle at depths of about 50 km and temperatures between 970–1030 °C. Their ultimate source is "asthenospheric", and they derive from a mildly depleted upper mantle, as indicated by their isotopic composition: $\varepsilon_{Sr} = -10.18$ to $-10.87$, $\varepsilon_{Nd} = 4.58$ to 5.73 and $^{206}Pb/^{204}Pb = 18.68$ to 19.18. The isotope ratios are interpreted as "asthenospheric" mixtures of depleted (DM) and enriched (HIMU) mantle components. From additional geological observations in the Southern-Alpine domain, we conclude that "active" mantle upwelling during the Anisian caused uplift, while volcanism and magmatism began later in Ladinian times. It is suggested that the alkaline dykes in the northern Ivrea zone are of Triassic age, as is the larger Monzoni intrusive complex further east, and that they are derivatives of the convecting asthenosphere.

*Keywords:* Southern Alps, magmatic rocks, plate tectonics, geodynamic setting, convecting asthenosphere.

## 1. Introduction

Since the late Carboniferous, the Southern-Alpine domain was an integral part of the growing supercontinent Pangea. This area was located at the southern edge of the European Variscan fold belt with continental and marine sedimentary deposits indicating a changing continental margin between Paleoeurope in the N and NW and an opening ocean in the SE (CASSINIS et al., 1988; BECHSTÄDT et al., 1978). Here, extensive magmatism occurred in the Late Carboniferous and Lower Permian with lesser degrees of magmatic activity in the Middle Triassic.

The magmatic rocks testify to the geodynamic evolution of the Southern Alps during Permo-Triassic times (Fig. 1), i.e. between the end of the Variscan orogeny and the initial breakup of Pangea. The latter event, finally, is documented by the Jurassic push of the Tethys ocean into Western Mediterranean regions indicating the separation of Gondwana from Laurussia (ZIEGLER, 1993a; FROITZHEIM et al., 1996). From west to east, the horst and graben structured Southern-Alpine

[1] Mineralogisches Institut, Universität Heidelberg, Im Neuenheimer Feld 236, D-69120 Heidelberg, FRG. <vstaehle@min.uni-heidelberg.de>
[2] Laboratorium für Geochronologie, Universität Heidelberg, D-69120 Heidelberg, FRG.
[3] Centre de Recherches Pétrographiques et Géochimiques, F-54501 Vandoevre, France.
[4] Mineralogisch-Petrographisches Institut, Universität Basel, CH-4056 Basel, Switzerland.
[5] Institut für Geologie und Paläontologie, Technische Universität Braunschweig, D-38106 Braunschweig, FRG.

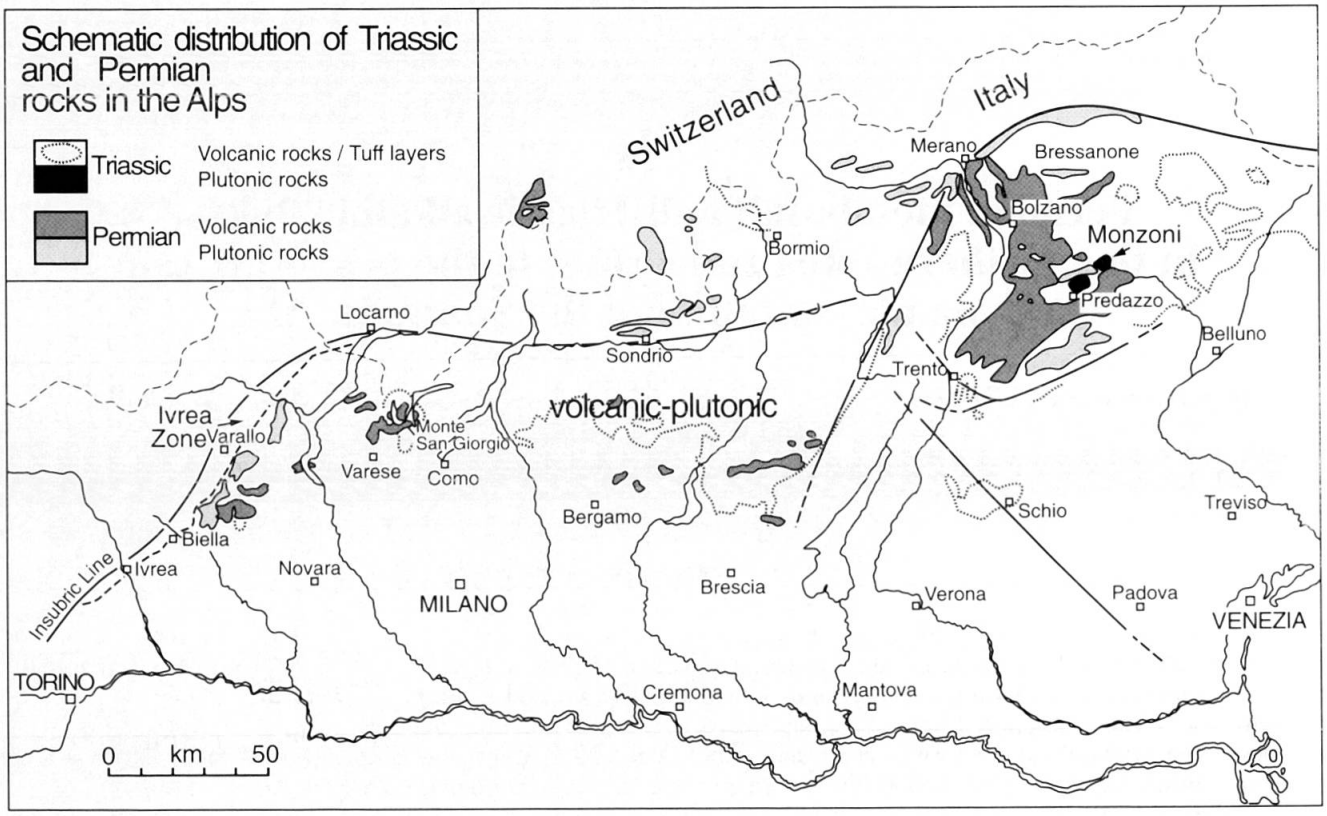


*Fig. 1* Distribution of the Triassic and Permian volcanic/plutonic rocks in the Southern Alps. The Ivrea zone lies southeast of the Insubric Line at the western termination of the Southern-Alpine region (after FIORENTINI POTENZA et al., 1975). The Lower Permian metagabbroic/metabasaltic rocks of the Ivrea zone are shown in figure 2.

basement, in part covered by Mesozoic and Cenozoic sediments, shows successively higher crustal positions, as indicated by the decreasing metamorphic grade of the basement rocks (VAI and COCOZZA, 1986).

The Ivrea zone at the western end of the Southern-Alpine domain (Fig. 1) is a small, highly eroded part of the crust. It is approximately 130 km long, is fault bounded and was uplifted between the Triassic and the Alpine collision and backfolding. Large quantities of peridotitic mantle rocks occur within granulite facies lower crustal rocks. The Finero, Balmuccia and Baldissero peridotite massifs are lined up along the western segment of the Neogene Insubric Line. Their present geological setting at the surface and the pronounced gravity anomaly found along strike, led to the assumption that the Ivrea zone is a rare example where the lower continental crust-upper mantle boundary outcrops at the surface (BERCKHEMER, 1969; FOUNTAIN and SALISBURY, 1981). Based on seismic and gravity studies along several geophysical traverses, the geophysical Ivrea body has been modeled as an upthrusted and tilted mantle wedge rising from the Adriatic mantle. This model was not unequivocally confirmed by the ECORS-CROP traverse (ECORS-CROP DEEP SEISMIC SOUNDING GROUP 1989; ROURE et al., 1990). Based on geological arguments, QUICK et al. (1995) and BORIANI and VILLA (1997) argued against the hypothesis that the Ivrea zone is a typical crust-mantle cross section. In this particular part of the Alps, in which the Adriatic and European plates are interlinked, many multidisciplinary studies have been carried out over the last 30 years (as reviewed by DAL PIAZ, 1993; GEBAUER, 1993; SCHMID et al., 1996; PFIFFNER et al., 1997, among others).

During the Permian, large volumes of basaltic magma (Mafic Formation, Fig. 2) intruded the lower crustal rocks of the Ivrea zone, probably after the peak of granulite-facies regional metamorphism (BARBOZA et al., 1999). During the same period, voluminous granitoid plutons (e.g. Baveno) and rhyolitic extrusives (e.g. Bozen region) were emplaced into more easterly parts of the Southern Alpine domain. Magmatic underplating of mafic mantle melts triggered the rise of these acidic melts (VOSHAGE et al., 1990). However, the geotectonic setting of the Permian magmatic rocks is controversial, being regarded either as arc-related (RIVALENTI et al., 1980; SCHENK,

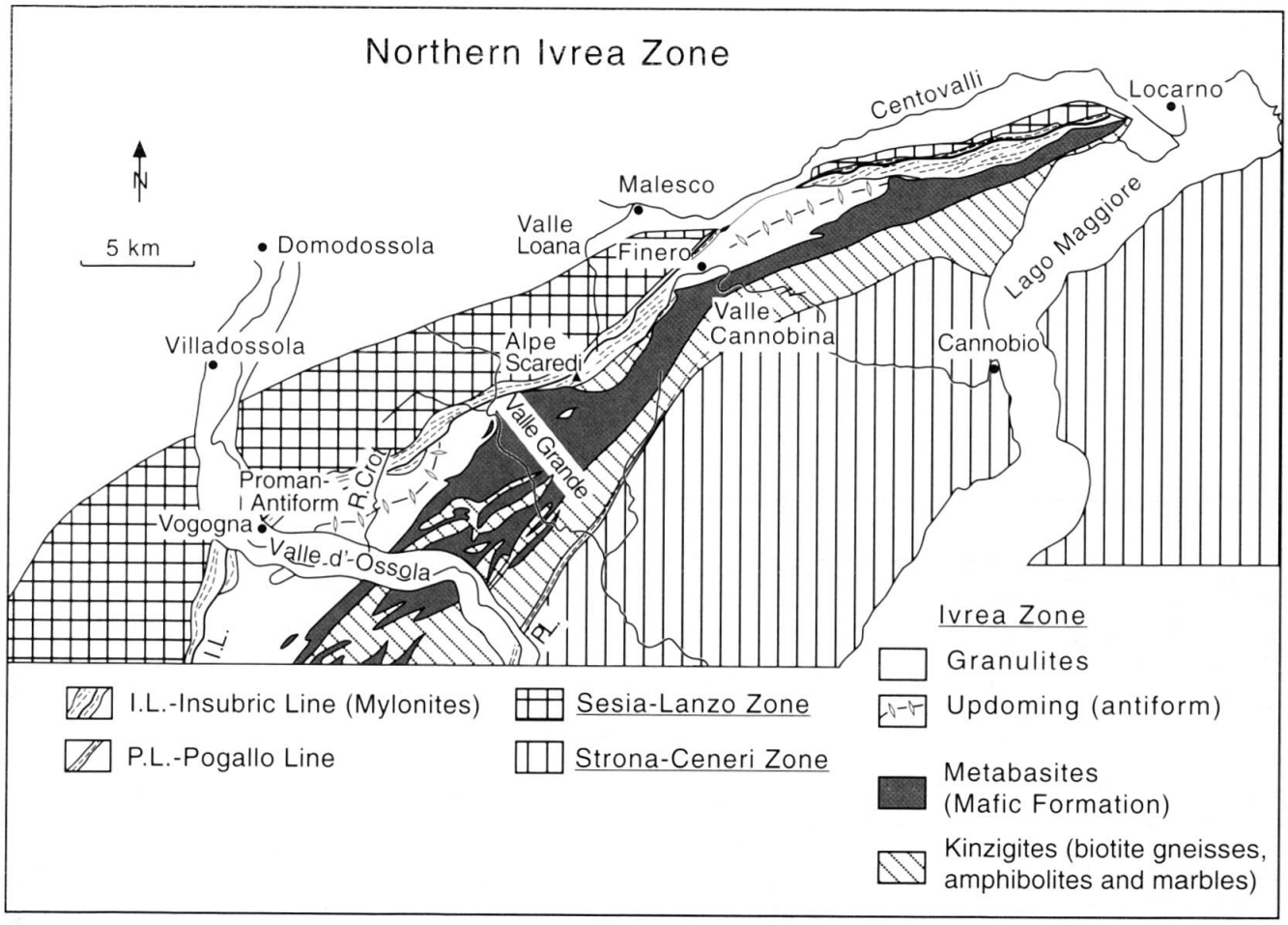


*Fig. 2* Geological sketch of the northern Ivrea zone. The Sesia-Lanzo zone north of the Insubric Line belongs to the Central Alps, whereas the Ivrea zone and the eastern Strona-Ceneri zone are part of the Southern-Alpine domain. The Finero and Proman antiform are updomed areas predominantly composed of granulite facies mafic and ultramafic rocks.

1981) or as products formed in a transtensional/extensional setting (HANDY and ZINGG, 1991; ROTTURA et al.,1997). Geodynamically, the strong Late-Paleozoic magmatism is seen by some as related to the beginning of the Alpine era (WOPFNER, 1984; DAL PIAZ and MARTIN, 1998), whereas STAMPFLI (1996) starts the "Tethyan cycle" (opening of the Alpine Tethys Central Atlantic system) no earlier than mid-Triassic, as did ZIEGLER (1993b) who introduced the term Permo-Triassic plate reorganization.

During the Triassic, alkaline dyke rocks were emplaced into the Ivrea zone. In general, the Southern-Alpine domain was dominated by explosive volcanism with regional scale tuff layers. This magmatism culminated in the emplacement of the 230 Ma old Monzoni intrusive complex (BORSI et al., 1968; Fig. 1). The geodynamic setting of this magmatism is keenly debated (e.g. DOGLIONI, 1987; CASTELLARIN et al., 1988; BONADIMAN et al., 1994), and the magmatism of Mt. Monzoni appears to contradict current concepts of plate tectonics (MASCH and HUCKENHOLZ, 1993). STAMPFLI (1996) related this event in the Ladinian/Carnian to the subduction of the Hallstadt-Meliata ocean in the east of the Adriatic plate, whereas BONADIMAN et al. (1994) inferred a model for the Triassic magmatism as having originated in a transcurrent geodynamic setting.

The basic question of when the "Alpine cycle" started and the controversy over the geodynamic context made a petrologic study of the Permian and Triassic magmatic rocks in the northern Ivrea zone worthwhile. These magmatic intrusions occur at a deep crustal level where differentiation and crustal contamination may be minor or absent, at least in some places. Secondly, this study aims to verify if these magmatic rocks are indeed connected with the geophysical Ivrea body, which was detected by seismic methods at shallow depths of about 5 to 10 km below the surface. Some of the geological surveys and early results of this study have been documented by STÄHLE (1991).

## 2. Geological setting of the magmatic rocks

Permo-Triassic magmatic rocks were studied in the northern Ivrea zone between Locarno and Valle d'Ossola (Fig. 2). Field studies focused on the areas near Finero and the upper Valle Grande, near the Insubric Line where granulite facies rocks were updomed by the Finero and Proman antiforms, respectively. The mafic-ultramafic complex at Finero, predominantly of gabbro and peridotite composition, has been investigated geologically and petrologically in detail over the last decades (for a review see LU et al., 1997a).

Permian metabasalts/metagabbros in the Finero area, which comprise the northern part of the main Mafic Formation, have a thickness of about 900 m. Bordered by the amphibole peridotite in the northwest and the Kinzigite Formation in the southeast, these voluminous mafic rocks (called External Gabbro in LU et al., 1997a) were studied along a section of the Cannobio-Finero road and

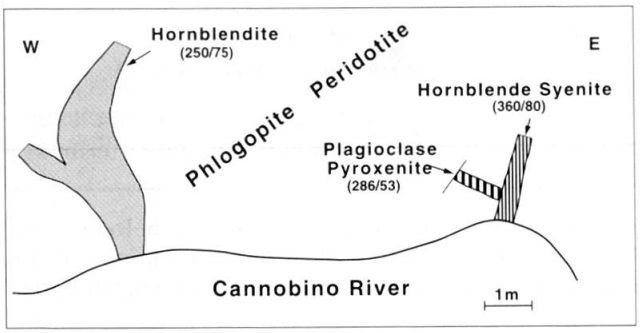


*Fig. 3* Geological sketch of pegmatitic alkaline dyke rocks in the phlogopite peridotite of Finero. Dykes occur at the northern bank of the Cannobino river near the Finero-Provola bridge. Figures in parentheses are dip directions and dip angles. (Swiss Topographic map 285 Domodossola: kilometric grid 106.45/684.75).

the nearby gorge of Valle Cannobina (Fig. 2). Numerous layers of steeply inclined meter-thick metapelitic stronalites and sedimentary metacarbonates are found within the Mafic Formation (STÄHLE, 1991).

Triassic zircon syenite pegmatites occur at Rio Creves (STÄHLE et al., 1990). Mafic and ultramafic, hornblende-rich dykes with variable feldspar contents were found in the Finero area and in the region of Val Fiorina (upper Valle Grande; Fig. 2). Farther south of Valle d'Ossola, further ultramafic hornblendite dykes occur. Two of them, an ultramafic hornblendite and a hornblende syenite, were studied. Both dykes show varying strike directions within the phlogopite peridotite south of Finero near the Finero-Provola bridge (Fig. 3). With regard to the age (but with some limitations, see chapter 5.7) and isotopic characteristics, they are related to the zircon syenite pegmatites (see chapter 5.5).

## 3. Analytical methods

Mineral compositions were determined using a fully automated JEOL JXA 8600 microprobe at the University of Basel. An acceleration voltage of 15 kV and a sample current of 10 nA were used (PROZA correction procedure). Analyses were made in wavelength dispersive energy mode (WDS) using a mix of synthetic and natural standards.

Major, minor and most trace elements of bulk rocks were determined by wavelength dispersive X-ray fluorescence spectroscopy at the University of Heidelberg and the CNRS Nancy. REE analyses of hand-picked apatite and calcite grains from a hornblendite dyke were performed by ICP-OES (University of Braunschweig).

Stable isotopic ratios $^{18}O/^{16}O$ and $^{13}C/^{12}C$ were measured using a VG-SIRA 9 mass spectrometer (University of Bonn). Analytical procedures are found in HOFFBAUER and SPIERING (1994).

Rb–Sr and Sm–Nd isotope ratios were measured using a VG Sector 54 mass spectrometer (University of Münster). 100 mg of the powdered and spiked samples were acid fluxed with a mix of concentrated $HF/HNO_3$. Rb–Sr and Sm–Nd were separated by chromatography. Absorption of Sm–Nd during the isolation process was performed in accordance with RICHARD et al. (1976). Calculations of the isotopic ratios and elemental concentrations were based on constants given by STEIGER and JÄGER (1977).

Lead isotopes $^{206}Pb$, $^{207}Pb$ and $^{208}Pb$ were measured in feldspars from syenitic dyke rocks using a Finnigan MS 261 thermal ion mass spectrometer (ETH Zürich). Sample preparation and analytical details are described by KÖPPEL et al. (1997).

The conventional K–Ar technique and the $^{40}Ar/^{39}Ar$ method were used on various hornblende separates obtained from a hornblende syenite and a hornblendite dyke. Analytical procedures were performed at the Laboratorium für Geochronologie, Universität Heidelberg. By applying the $^{40}Ar/^{39}Ar$ method by step heating, argon distortions due to $^{40}Ar$ excess could be detected. Sample preparations and analytical procedures are described by HESS et al. (1995).

## 4. Petrography and geochemistry of Permian metabasalts (Mafic Formation)

Granulite-facies metabasalts or metagabbros, recovered from the SE–NW Cannobino cross section (C31-C360/1; Tab. 1), are dark coloured, medium-grained, massive rocks. The magmatics consist of gabbros, hornblende gabbros and more rarely of gabbronorites. In the vicinity of the amphibole peridotite the magmatics are layered whereas downstream in the Cannobino gorge the metagabbros are predominantly massive and homogeneous. No mantle xenoliths were found within these metagabbroic rocks. The metagabbros are voluminous magmatic intrusions into lower crustal country rocks (VOSHAGE et al., 1990). However, a syn- to posttectonic strong mylonitic overprinting has obliterated any primary igneous textures.

Main mineral constituents are hornblende, clinopyroxene and plagioclase. The hornblende grains are inequigranular, elongated or oval in shape and display a distinct olive-brown to light yellow pleochroism. Some of the feldspars have bent twin lamellae, and plagioclase frequently shows strong grain-reduced recrystallization due to intense mylonitic shearing. Colourless, equigranular, diopsidic pyroxene is found throughout the studied area, whereas pink orthopyroxene and mm-sized, isometric almandine garnet are present only in some of the studied samples. Biotite occurs only on a local scale, and accessory phases include sphene, apatite and zircon. The opaques are anhedral, titaniferous magnetite and ilmenite showing twin lamellae.

The studied rock samples are massive and unweathered but some show, in parts, evidence of low-temperature alteration, mainly along grain boundaries or along mineral fractures in clinopyroxene and/or plagioclase.

Along small fissures and in local zones of fluid circulation in rocks of the Mafic Formation, variable quantities of epidote/clinozoisite, chlorite, actinolite, sericite, calcite, pyrite and chalcopyrite occur as secondary alteration products. These are associated with greenschist facies metamorphism, probably of Alpine age.

The chemical composition of 13 samples of metagabbroic rocks from the Finero area is shown in table 1. Analyzed samples in the present

*Tab. 1* Chemical composition of metabasalts from the cross section of the Valle Cannobina.

| | C31 | C12 | C48 | C358 | C355 | C353a | C353b | C43 | C350 | C360 | C360a | C360b | C360/1 |
|---|---|---|---|---|---|---|---|---|---|---|---|---|---|
| | | | | | | *Major oxide abundances [wt%]* | | | | | | | |
| $SiO_2$ | 48.34 | 44.93 | 45.09 | 42.57 | 45.04 | 44.38 | 40.46 | 45.57 | 44.07 | 45.40 | 45.45 | 43.18 | 43.80 |
| $TiO_2$ | 1.09 | 1.80 | 2.43 | 2.93 | 2.63 | 3.78 | 2.71 | 2.70 | 2.89 | 2.18 | 2.19 | 3.16 | 2.89 |
| $Al_2O_3$ | 13.88 | 13.67 | 13.43 | 12.68 | 13.15 | 12.14 | 15.74 | 13.40 | 12.28 | 31.89 | 13.36 | 13.01 | 13.20 |
| $Fe_2O_3$* | 4.09 | 4.47 | 4.70 | 4.78 | 4.33 | 5.28 | 4.64 | 4.80 | 5.45 | 4.24 | 4.02 | 5.13 | 5.24 |
| FeO | 7.78 | 9.46 | 10.07 | 12.92 | 9.81 | 12.43 | 11.14 | 10.36 | 12.26 | 9.76 | 9.39 | 11.87 | 11.39 |
| MnO | 0.13 | 0.21 | 0.21 | 0.29 | 0.18 | 0.28 | 0.18 | 0.21 | 0.28 | 0.21 | 0.24 | 0.24 | 0.23 |
| MgO | 10.17 | 8.78 | 7.97 | 7.17 | 9.33 | 7.40 | 9.03 | 7.79 | 7.94 | 6.53 | 6.81 | 8.41 | 8.13 |
| CaO | 10.10 | 12.79 | 12.75 | 13.08 | 10.92 | 10.51 | 11.06 | 11.89 | 10.04 | 13.11 | 13.88 | 10.71 | 10.55 |
| $Na_2O$ | 2.91 | 2.22 | 2.43 | 0.84 | 1.74 | 1.78 | 2.07 | 2.42 | 2.09 | 1.79 | 1.71 | 2.02 | 2.55 |
| $K_2O$ | 0.37 | 0.58 | 0.24 | 0.12 | 0.40 | 0.14 | 0.38 | 0.06 | 0.30 | 0.14 | 0.08 | 0.31 | 0.24 |
| $P_2O_5$ | 0.18 | 0.14 | 0.23 | 0.23 | 0.33 | 0.32 | 0.12 | 0.24 | 0.36 | 0.15 | 0.15 | 0.27 | 0.30 |
| LOI | 0.56 | 0.26 | 0.31 | 1.40 | 1.89 | 1.17 | 1.39 | 0.17 | 1.23 | 0.94 | 0.69 | 1.06 | 1.30 |
| Total | 99.60 | 99.31 | 99.86 | 99.01 | 99.75 | 99.61 | 98.92 | 99.61 | 99.19 | 98.34 | 97.97 | 99.37 | 99.82 |
| mg#[a] | 63.7 | 56.3 | 52.5 | 45.2 | 57.3 | 46 | 53.9 | 51.2 | 47.8 | 49.8 | 50.9 | 50.3 | 50 |
| | | | | | | *Trace element abundances [ppm]* | | | | | | | |
| Rb | 5.0 | 6.0 | 3.0 | 5.0 | 3.0 | 4.5 | 7.0 | 3.0 | 4.0 | 4.0 | 3.0 | 5.5 | 4.4 |
| Ba | 90.0 | 29.0 | 24.0 | 37.0 | 284.0 | 70.0 | 114.0 | 26.0 | 68.0 | 44.0 | 37.0 | 71.0 | 133.0 |
| La | 22.0 | 3.0 | 1.0 | 5.4 | 9.0 | 5.0 | 7.0 | 26.0 | 16.0 | 1.0 | 1.0 | 4.0 | 5.5 |
| Ce | 43.0 | 33.0 | 26.0 | 17.0 | 63.0 | 20.0 | 29.0 | 18.0 | 22.0 | 12.0 | 20.0 | 29.0 | 20.1 |
| Sr | 220.0 | 439.0 | 105.0 | 115.0 | 317.0 | 148.0 | 398.0 | 184.0 | 263.0 | 195.0 | 161.0 | 146.0 | 109.0 |
| Nb | 12.0 | 13.0 | 3.0 | 5.0 | 28.0 | 4.0 | 8.0 | 7.0 | 11.0 | 4.0 | 3.0 | 8.0 | 5.3 |
| Zr | 78.0 | 256.0 | 123.0 | 135.0 | 149.0 | 188.0 | 51.0 | 259.0 | 178.0 | 131.0 | 136.0 | 172.0 | 218.0 |
| Y | 14.0 | 29.0 | 35.0 | 41.0 | 21.0 | 45.0 | 19.0 | 42.0 | 43.0 | 37.0 | 45.0 | 44.0 | 55.3 |
| Cr | 411.0 | 201.0 | 236.0 | 124.0 | 265.0 | 111.0 | 97.0 | 190.0 | 116.0 | 235.0 | 247.0 | 154.0 | 133.0 |
| Ni | 256.0 | 247.0 | 73.0 | 67.0 | 198.0 | 60.0 | 30.0 | 145.0 | 48.0 | 82.0 | 66.0 | 71.0 | 65.4 |

*FeO and $Fe_2O_3$ is calculated after LE MAITRE (1976).
[a]mg# = $100MgO/(MgO + 0.9FeO_{tot})$, mean mg# = 51.9.

study were taken to avoid such hydrothermal alterations as far as possible. Chemically these rocks resemble MORB-type basalts (STÄHLE, 1991). Compared to average MORB, the metagabbros of the Mafic Formation have somewhat lower amounts of $SiO_2$ and higher $FeO_{tot}$ and $TiO_2$. Their normalized trace element patterns reveal that these mafic rocks represent ordinary gabbros of the original liquid composition. This is in contrast to the cumulitic nature of the adjacent Internal Gabbro and the Amphibole Peridotite (LU et al., 1997a).

Normatively classified as olivine tholeiites (CIPW), the metagabbros of the Mafic Formation have anomalously low mg#-values in the range of 64 to 45, with an average of 51.9 (Tab. 1).

The compositional variation of 3 metabasalts is shown on a spiderdiagram in figure 4. Compared to N-type MORB, most elements in the diagram are arranged subparallel to the MORB line in accordance with LU et al. (1997a). However, the highly incompatible elements Rb and Ba are somewhat enriched, possibly due to secondary alteration. A trough is seen at K, La, and maxima are reached at Ti and Fe. This could be due to mineral accumulations, and the latter enrichments may be traced to fractionation of mg-rich minerals. Nb levels are variable, but do not show negative peaks in the graphs as indication of a subduction-related origin. The compatible elements Cr and Ni are visibly depleted due to the fractionation of olivine, clinopyroxene and possibly Cr-spinel. Thus, the elemental relationships fit those of highly fractionated continental basalts (see chapter 6.1).

## 5. Petrography, geochemistry, isotope studies and geochronology of the Triassic dyke rocks

### 5.1. PETROGRAPHY OF THE HORNBLENDITE AND HORNBLENDE SYENITE DYKE

The hornblendite and hornblende syenite dyke samples consist mainly of hornblende with different amounts of plagioclase of a very narrow compositional range ($An_{08-13}$). The dykes are pegmatites with coarse-grained textures.

The nearly vertical hornblendite dyke in the phlogopite peridotite (Fig. 3) is approximately 1 m in thickness, very dark in colour, and shows a very high luster. A 2 cm thick border of greenish clinopyroxene formed by reaction with the peridotite country rock. Twinned calcite, as a primary matrix mineral among coarse-grained hornblende, is unevenly distributed within the dyke. The estimated contents are 3–5 vol%. Brown to pale yellow, kaersutitic hornblende makes up 90 vol% of the rock. Fine-grained, rarely twinned albite, platy red-brown pleochroic biotite, light-green clinopyroxene, and round or euhedral apatite grains are present in the interstices of hornblende. Many hornblende crystals, with grain sizes of up to 3 cm, appear rounded due to corrosion, with albite or calcite replacement at the edges. Accessory minerals include magnesium-poor ilmenite (MgO ≈ 0.5 wt%), magnetite and chalcopyrite.

The hornblende syenite dyke is about 35 cm thick, steeply inclined and strikes east–west (Fig. 3). The dyke crystallized at a late stage of the complex evolution under increasing, north–south-ori-

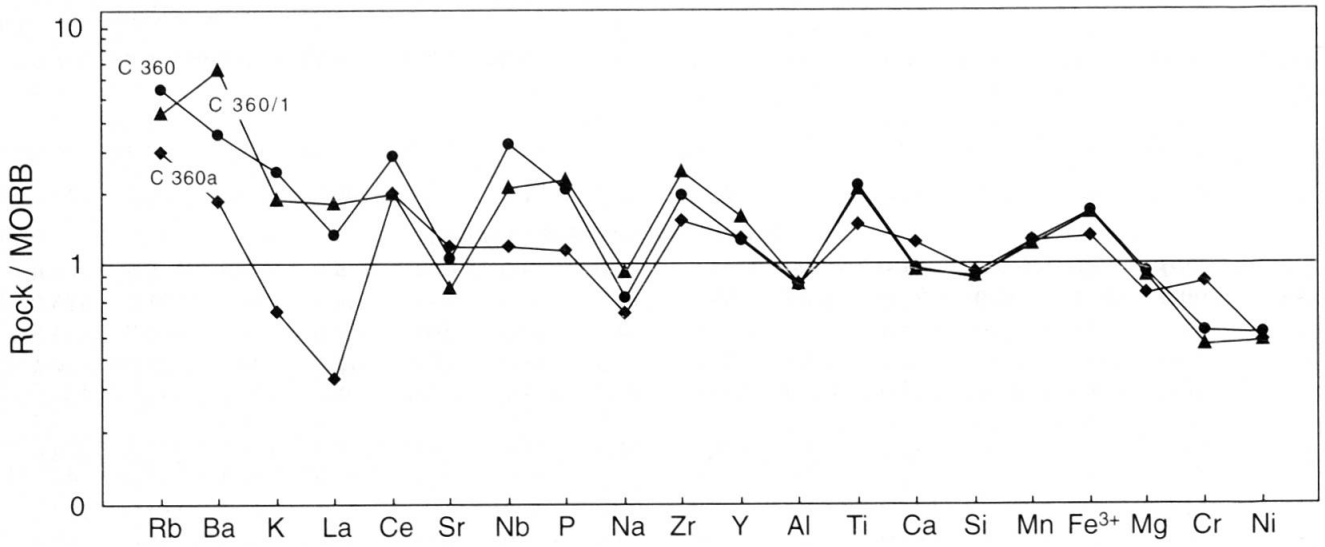


*Fig. 4* N-type MORB normalized spidergram of the metabasalts C360, C360a and C360/1. Note the distinct Ni and Cr depletion. Standardisation values of N-type MOR-basalts from STÄHLE (1991).

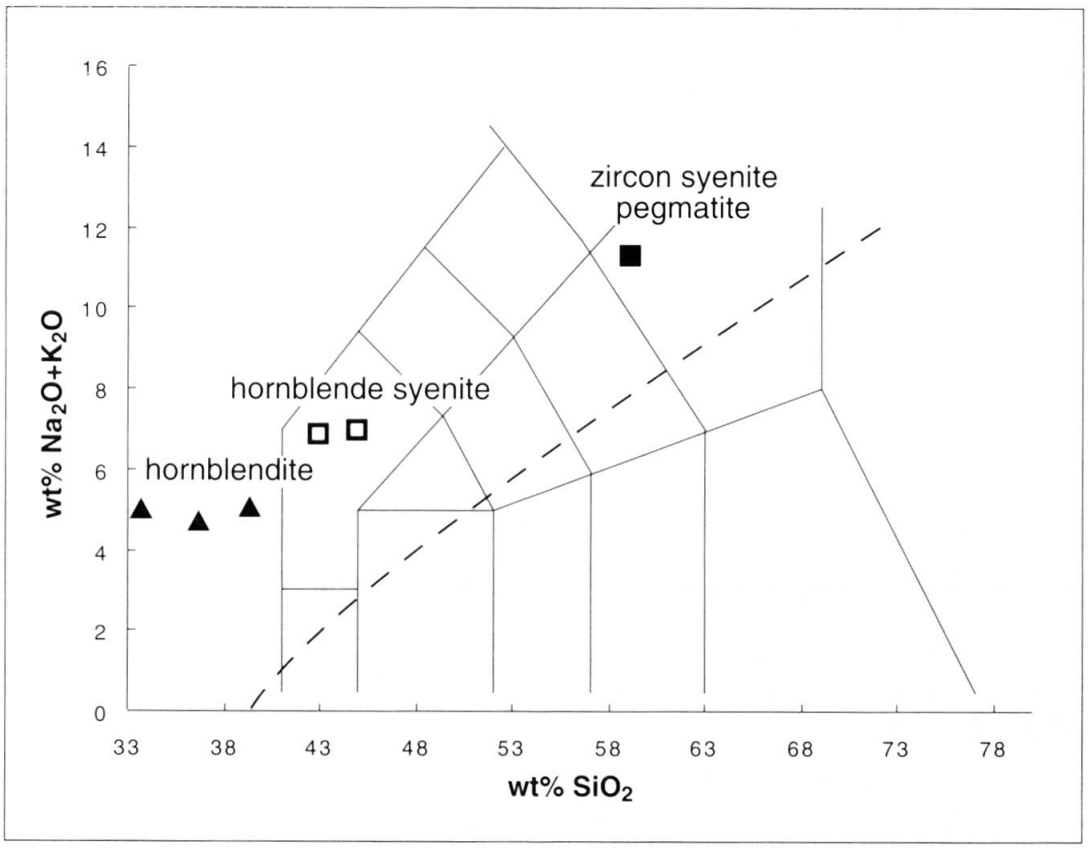


*Fig. 5* Total alkali silica diagram (LE MAITRE, 1989) for hornblendite dyke, hornblende syenite and zircon syenite pegmatite. The dashed line (IRVINE and BARAGAR, 1971) divides alkaline from subalkaline magmatic rocks..

ented stress conditions. The major compressive force was approximately north–south and imprinted a mylonitic fabric on the rock. The dyke is dominated by untwinned masses of oligoclase with plaster fabrics that enclose rounded cm-size pargasitic-kaersutitic hornblende clasts. Amphibole is elongated parallel to strike, forming tails and boudins. Calcite and opaques grew in pressure shadows of hornblende, presumably assisted by late magmatic fluids. Foxy-red, pleochroic biotite partially replaces hornblende at late stages of crystallization, and occasional, xenomorphic sodalite underlines the alkalic character of the dyke. Rare, greenish to pink pleochroic clinopyroxene is locally replaced by hornblende, and tiny crystals of accessory zircon also occur.

## 5.2. CHEMICAL COMPOSITON OF THE DYKES AND SOME OF THEIR MINERALS

The bulk rock chemistry of the unaltered pegmatite dykes shows that the hornblendite has the lowest silica and highest iron contents (Tab. 2). Due to calcite-rich segregations, the specimens of the hornblendite dyke were subdivided into $CaCO_3$-poor (C485, C550a) and $CaCO_3$-rich (C550, C551) samples. High $CaCO_3$ samples also contain high levels of phosphorous. Because apatite crystals are found mostly co-existing with the calcite matrix. Hornblende syenite has an intermediate chemical composition, and the zircon syenite pegmatite has the highest silica and alkali contents. All dykes are alkaline (Fig. 5) and are characterized by higher sodium than potassium levels.

The mg#-values for the hornblendite dyke range from 53 to 62 (Tab. 2), indicating fractionation processes. The mg#-number of 77 for the zircon syenite pegmatite may reflect a primary upper mantle source (FREY et al., 1978).

In comparison to average crustal rocks, the dykes show high levels of niobium, tantalum, strontium, zirconium, and lower levels of rubidium, lead, uranium, thorium (Tab. 2). The zircon syenite pegmatite (sample 39; some 5 cm in size) has very high Zr and low Y contents. However, compositional variations may exist due to unequal distribution of larger zircon crystals (size ≤1 cm) within these feldspar-rich, pegmatitic rocks.

Rare earth element concentrations (Tab. 2) show that the highest levels are in the $CaCO_3$-rich

*Tab. 2* Major element, trace element and rare earth element contents of a hornblendite, a hornblende syenite and a zircon syenite pegmatite shown in figure 3. The hornblende syenite (sample C377) is from Val Fiorina and the zircon syenite pegmatite (sample 39) from Rio Creves (STÄHLE et al., 1990).

| | Hornblendite ($CaCO_3$-poor) | Hornblendite ($CaCO_3$-poor) | Hornblendite ($CaCO_3$-rich) | Hornblendite ($CaCO_3$-rich) | Hornblende syenite | Hornblende syenite | Zircon syenite pegmatite |
|---|---|---|---|---|---|---|---|
| | C485 | C550a | C550 | C551 | C557 | C377 | 39 |
| | | | | *Major oxide abundances [wt%]* | | | |
| $SiO_2$ | 36.17 | 38.86 | 32.87 | 26.79 | 42.25 | 44.71 | 57.98 |
| $TiO_2$ | 1.96 | 2.21 | 1.50 | 1.49 | 1.33 | 1.00 | 0.27 |
| $Al_2O_3$ | 12.05 | 13.10 | 11.18 | 9.10 | 14.62 | 15.12 | 20.83 |
| $Fe_2O_3$* | 14.94 | 18.35 | 11.94 | 11.94 | 11.49 | 10.46 | 2.35 |
| MnO | 0.22 | 0.27 | 0.20 | 0.21 | 0.15 | 0.20 | 0.00 |
| MgO | 9.92 | 9.56 | 8.98 | 6.89 | 6.65 | 4.48 | 3.62 |
| CaO | 14.34 | 10.42 | 17.33 | 24.37 | 10.92 | 11.71 | 1.62 |
| $Na_2O$ | 3.32 | 3.67 | 2.93 | 2.49 | 4.86 | 4.87 | 9.01 |
| $K_2O$ | 1.38 | 1.33 | 2.00 | 1.05 | 1.98 | 2.10 | 2.12 |
| $P_2O_5$ | 1.36 | 0.35 | 1.90 | 3.16 | 0.73 | 0.12 | 0.15 |
| $CO_2$ | 3.02 | 0.81 | 7.21 | 11.09 | 3.72 | 4.89 | 0.16 |
| S | 0.03 | 0.02 | 0.02 | 0.14 | 0.02 | 0.12 | 0.04 |
| $H_2O$ | 1.94 | 1.99 | 2.19 | 1.45 | 1.58 | 1.08 | 1.26 |
| Total | 100.65 | 100.94 | 100.25 | 100.17 | 100.30 | 100.86 | 99.41 |
| mg# [a] | 59.4 | 53.4 | 62.3 | 55.9 | 56 | 48.5 | 77.3 |
| | | | | *Trace element abundances [ppm]* | | | |
| Rb | 15.50 | 14.40 | 44.20 | 12.10 | 23.70 | 15.90 | 57.30 |
| Ba | 340.00 | 362.00 | 788.00 | 380.00 | 663.00 | 645.00 | 1128.00 |
| Th | 1.64 | 0.48 | 2.17 | 3.18 | 0.99 | 1.08 | 2.50 |
| U | 0.53 | 0.14 | 0.38 | 0.69 | 0.23 | 0.12 | 0.83 |
| Ta | 10.20 | 11.90 | 7.55 | 6.93 | 7.89 | 8.23 | 9.54 |
| Nb | 167.00 | 194.00 | 129.00 | 121.00 | 120.00 | 135.00 | 79.20 |
| Sr | 1649.00 | 848.00 | 3196.00 | 4071.00 | 2674.00 | 2221.00 | 2256.00 |
| Zr | 423.00 | 461.00 | 285.00 | 283.00 | 316.00 | 318.00 | 798.00 |
| Y | 56.80 | 31.00 | 85.30 | 117.00 | 43.40 | 35.90 | 2.57 |
| Pb | 3.19 | 4.10 | 2.56 | 7.46 | 3.07 | 2.73 | 14.80 |
| Sc | 14.10 | 12.50 | 13.60 | 14.70 | 11.00 | 14.10 | 2.50 |
| V | 61.40 | 65.50 | 48.70 | 43.90 | 42.30 | 114.00 | 9.58 |
| Cr | 22.30 | 60.10 | 197.00 | 23.70 | 92.50 | 81.30 | 11.40 |
| Co | 34.10 | 33.30 | 35.00 | 32.60 | 31.80 | 28.80 | 23.40 |
| Cu | 38.80 | 162.00 | 61.50 | 109.00 | 29.90 | 34.20 | 13.20 |
| Ni | 273.00 | 203.00 | 311.00 | 185.00 | 169.00 | 62.10 | 136.00 |
| Zr/Nb | 2.53 | 2.38 | 2.21 | 2.34 | 2.63 | 2.36 | 10.08 |
| | | | | *Rare earth element abundances [ppm]* | | | |
| La | 82.20 | 81.00 | 144.60 | 205.50 | 59.30 | 61.00 | 6.25 |
| Ce | 174.40 | 51.10 | 276.90 | 383.40 | 122.80 | 113.50 | 10.30 |
| Pr | 20.10 | 7.39 | 31.70 | 46.00 | 14.20 | 12.60 | 1.04 |
| Nd | 79.80 | 32.10 | 128.20 | 188.00 | 57.00 | 47.90 | 3.67 |
| Sm | 15.50 | 7.30 | 23.00 | 33.00 | 11.10 | 8.68 | 0.83 |
| Eu | 5.23 | 2.71 | 7.00 | 9.72 | 3.72 | 2.79 | 0.53 |
| Gd | 13.90 | 6.76 | 20.40 | 29.20 | 10.30 | 7.51 | 0.59 |
| Tb | 2.13 | 1.13 | 2.83 | 3.98 | 1.49 | 1.08 | 0.10 |
| Dy | 10.80 | 6.10 | 15.30 | 21.20 | 8.16 | 6.21 | 0.59 |
| Ho | 2.11 | 1.19 | 3.29 | 4.52 | 1.71 | 1.31 | 0.12 |
| Er | 5.31 | 3.03 | 7.65 | 10.70 | 4.01 | 3.25 | 0.30 |
| Tm | 0.80 | 0.47 | 1.09 | 1.50 | 0.59 | 0.49 | 0.06 |
| Yb | 4.69 | 2.92 | 6.99 | 9.74 | 3.96 | 3.27 | 0.40 |
| Lu | 0.71 | 0.43 | 1.01 | 1.44 | 0.59 | 0.46 | 0.08 |
| (La/Yb)cn | 27.1 | 9.6 | 32.0 | 32.6 | 23.2 | 28.8 | 24.2 |

*Total Fe as $Fe_2O_3$

[a] mg# = $100MgO/(MgO+0.9FeO_{tot})$

hornblendite samples with their large contents of apatite. The elemental abundances and the REE patterns indicate that the hornblendite dyke crystallized from a fractionated kimberlitic/carbonatitic magma (WASS et al., 1980).

Any carbonate in the hornblendite dyke is of primary, magmatic origin as indicated by its isotopic composition (see chapters 5.4 and 5.5). The calcite matrix of the dyke is homogeneous and is characterized by low MgO and FeO contents (Tab. 3) similar to the chemical composition of calcite minerals in calcio-carbonatites. Their high Ca/(Ca+Mg+Fe+Mn+Na) ratio of 0.96 points to a primary carbonate phase originating at a higher level in the upper mantle at about ≥1.5 GPa pressure or at a depth of ≥ 50 km (DALTON and WOOD, 1993; KOGARKO et al., 1995). Prior to melting, the source of the hornblendite dyke must have been altered by carbonatite metasomatism. Apatite in the dyke has higher contents of fluorine than chlorine (Tab. 3), and their Mn and Sr contents are typical of carbonatitic apatite (HOGARTH, 1989).

*Tab. 3* Selected electron microprobe analyses of calcite and apatite from the hornblendite dyke. Minerals were analyzed with electron microprobe (spot size 3 μm).

| | calcite C551a | calcite C551a | calcite C551a |
|---|---|---|---|
| MgO | 1.32 | 1.14 | 0.99 |
| MnO | 0.32 | 0.29 | 0.33 |
| FeO* | 1.01 | 1.11 | 0.80 |
| CaO | 53.30 | 52.75 | 52.62 |
| SrO | 1.07 | 0.95 | 1.01 |
| $Na_2O$ | 0.02 | 0.01 | 0.02 |
| Total | 57.04 | 56.25 | 55.77 |
| Number of ions on the basis of | 12(O) | 12(O) | 12(O) |
| Mg | 0.129 | 0.113 | 0.100 |
| Mn | 0.018 | 0.016 | 0.019 |
| Fe | 0.056 | 0.062 | 0.045 |
| Ca | 3.755 | 3.770 | 3.796 |
| Sr | 0.041 | 0.037 | 0.040 |
| Na | 0.002 | 0.002 | 0.002 |
| | 4.001 | 4.000 | 4.002 |
| Ca/(Ca+Mg+Fe+Mn+Na) = | 0.95 | 0.96 | 0.96 |

| | apatite C551a | apatite C551a | apatite C551a |
|---|---|---|---|
| FeO* | 0.25 | 0.21 | 0.18 |
| MnO | 0.10 | 0.10 | 0.04 |
| MgO | 0.09 | 0.05 | 0.06 |
| CaO | 53.87 | 54.16 | 53.95 |
| SrO | 0.79 | 0.81 | 0.87 |
| $P_2O_5$ | 41.87 | 41.11 | 41.99 |
| F | 1.05 | 1.45 | 1.28 |
| Cl | 0.37 | 0.29 | 0.31 |
| Total | 98.39 | 98.18 | 98.68 |
| Number of ions on the basis of | 25(O) | 25(O) | 25(O) |
| P | 6.019 | 5.966 | 6.024 |
| Fe | 0.036 | 0.030 | 0.026 |
| Mn | 0.014 | 0.014 | 0.006 |
| Mg | 0.022 | 0.012 | 0.015 |
| Cu | 9.801 | 9.948 | 9.796 |
| Sr | 0.078 | 0.080 | 0.086 |
| | 9.951 | 10.084 | 9.929 |
| F | 0.563 | 0.787 | 0.686 |
| Cl | 0.106 | 0.085 | 0.090 |

*Total Fe as FeO

## 5.3. REE CONTENTS OF APATITE AND MATRIX CALCITE FROM THE HORNBLENDITE DYKE

REE concentrations of apatite and calcite (Tab. 4) for the hornblendite dyke were determined for hand-picked crystals separated under the binocular. Apatite shows steep LREE-enriched patterns with high chondrite-normalized Lanthanum/Ytterbium ratios of 26–27. The La values are 3500–4300 times higher than standard chondrite, quite similar to those found for apatite in mantle xenoliths (WASS et al., 1980). Apatite has the highest concentration of REE among all minerals contained in the hornblendite dyke. Therefore, the occurrence of significant modal apatite within a sample will give a steep LREE pattern in the whole rock analysis (Tab. 2).

Chondrite-normalized REE patterns of separated calcite grains (Fig. 6) lie within the field defined by carbonatite rocks (CULLERS and GRAF, 1984). It is probable that the calcite separate is contaminated with 1–2% apatite and/or albite grains. Thus, the absolute REE concentrations may be elevated to some extent. However, the kinked slope of the calcite REE-curves is striking and significant. The LREE patterns have steep gradients, typical of those from carbonatites, whereas the HREE do not. The near horizontal path of the HREE curves cause Yb and Lu to lie above the field defined by carbonatites (samples C531, C550/2, C551 in figure 6). This pattern may indicate that the upper mantle source of the carbonate or the hornblendite dyke, respectively, contained little or no garnet. Such a curved pattern for the REE was first found in "oceanic" carbonatites (ALLÈGRE et al., 1971; LE BAS, 1984, Fig. 6) and distinguish oceanic from continental carbonatites.

*Tab. 4* Rare earth element abundances of separated apatite and calcite grains from hornblendite (ppm). The mortar-crushed mineral grains were separated under the binocular (weight of single separates 3–10 mg).

| | Ap C550 | Ap C535 | Cc C531 | Cc C550/2 | Cc C551 | Cc C550/1 |
|---|---|---|---|---|---|---|
| La | 1450.6 | 1188.2 | 521.7 | 246.6 | 183.0 | 132.7 |
| Ce | 3042.4 | 2482.6 | 1005.5 | 444.9 | 328.7 | 266.3 |
| Pr | 329.2 | – | – | 47.2 | 32.7 | – |
| Nd | 1212.5 | 1016.7 | 397.4 | 185.6 | 136.1 | 111.0 |
| Sm | 204.3 | 190.6 | 80.6 | 32.1 | 23.0 | 21.5 |
| Eu | 57.4 | 50.6 | 20.6 | 12.4 | 6.72 | 6.57 |
| Gd | 165.1 | 137.8 | 47.0 | 28.1 | 19.2 | 15.8 |
| Tb | 24.3 | 27.4 | 7.76 | 4.70 | 3.38 | 2.59 |
| Dy | 122.4 | 106.3 | 46.7 | 28.8 | 21.3 | 15.8 |
| Ho | 25.0 | – | – | 7.27 | 5.49 | – |
| Er | 51.8 | 41.1 | 23.6 | 18.0 | 12.8 | 7.40 |
| Tm | 6.51 | 4.67 | 3.36 | 2.78 | 1.92 | 1.02 |
| Yb | 36.1 | 28.2 | 21.3 | 17.8 | 12.5 | 6.35 |
| Lu | 4.34 | 3.86 | 3.46 | 3.05 | 1.90 | 1.00 |
| (La/Yb)cn | 26 | 27.3 | 15.8 | 8.95 | 9.5 | 13.5 |

## 5.4. $\delta^{13}C$ AND $\delta^{18}O$ STABLE ISOTOPIC COMPOSITION OF MATRIX CALCITE IN THE HORNBLENDITE DYKE

Analyzed carbonate separates of matrix calcite from different samples of the hornblendite dyke show $\delta^{13}C$ and $\delta^{18}O$ values ranging from – 5.93 to – 6.65 ‰ and 9.23 to 15.18 ‰, respectively (Tab. 5). The narrow range of $\delta^{13}C$ is typical of mantle derived carbon, and the $\delta^{18}O$ values of some calcite separates, also lie within the "magmatic" carbonatite box (see Fig. 7).

The $\delta^{13}C$ values show that calcite from the hornblendite dyke preserves the primary carbon isotope mantle signature. The $\delta^{13}C$ values, ranging from –5 to –7‰, characterize mantle-carbon reservoirs, as well as most ocean island and mid-ocean ridge basalts (Fig. 7; KELLER and HOEFS, 1995).

However, the majority of $\delta^{18}O$ values for the calcites are distinctly higher and lie outside the field of primary, igneous carbonatites. Higher val-

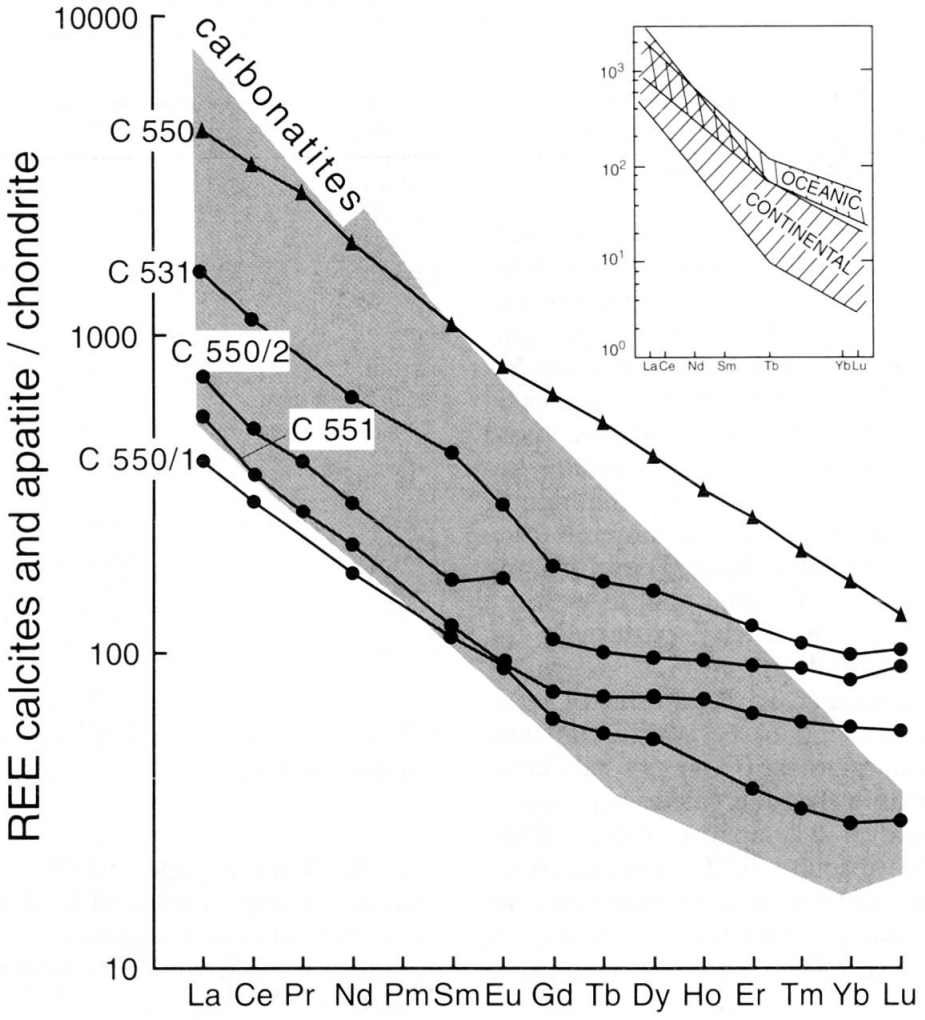


*Fig. 6* Chondrite-normalized REE distributions of calcite (•) and apatite (▲) separated from the hornblendite dyke (normalization see STÄHLE, 1991). The carbonate field represents REE contents found in most carbonatites (CULLERS and GRAF, 1984). Fields of oceanic and continental carbonatites shown in inset (after LE BAS, 1984).

ues in stable isotope composition of magmatic carbonate, particularly in $\delta^{18}O$, are commonly interpreted as being due to alteration processes and secondary isotope exchange (HUBBERTEN et al., 1988). The shift to higher $\delta^{18}O$ values observed in parts of the calcite separates from the dyke (Fig. 7) are primarily due to secondary exchange with meteoric waters.

## 5.5. SR AND ND ISOTOPIC COMPOSITION OF THE HORNBLENDITE DYKE (WHOLE ROCK) AND OF APATITE AND CALCITE FROM THIS DYKE

Sr–Nd isotope ratios for the hornblendite (whole rock) and for separated calcite and apatite grains from the dyke are presented in table 6 together with isotopic data from the 225 Ma old zircon syenite pegmatite.

The initial ratios of $^{87}Sr/^{86}Sr$ only show small variations in the range of 0.70364 to 0.70372. The initial ratios of $^{143}Nd/^{144}Nd$ also have a small spread from 0.512578 to 0.512642. The initial ratios in the $\varepsilon(t)$ notation, with t being taken as 225 Ma, are given in table 6.

In the $\varepsilon_{Sr}(t)$–$\varepsilon_{Nd}(t)$ correlation diagram of figure 8 both dyke rocks and the apatite and calcite separates of the hornblendite dyke form a tight cluster within the "mantle array". This means that the ultimate source of the dykes is "asthenospheric" (STÄHLE et al., 1996) and that the dykes show no crustal contamination in these isotopic ratios. Furthermore, the isotopic signatures and the LREE enriched pattern of the alkaline dykes reveal that the dykes represent small-volume melts derived from a slightly depleted upper mantle which was previously metasomatized by volatile-rich fluids or melts. Furthermore, isotopic evidence suggests that apatite, calcite and the hornblendite as a whole were derived from the same source in the mantle.

*Tab. 5* Carbon and oxygen isotopic composition from separates of matrix calcites from different samples of a hornblendite dyke.

| sample No. | $\delta^{18}O_{/SMOW}$ | $\delta^{13}C_{/PDB}$ |
|---|---|---|
| C488 | 14.11 | –6.55 |
| C489 | 15.18 | –6.44 |
| C500 | 9.66 | –6.10 |
| C531 | 19.45 | –6.60 |
| C533 | 11.31 | –6.65 |
| C535 | 13.75 | –5.93 |
| C549 | 10.30 | –6.42 |
| C550 | 9.23 | –6.43 |
| C550/1 | 10.27 | –6.34 |
| C551 | 10.59 | –6.02 |
| C553 | 9.23 | –6.43 |

Lying outside the strongly depleted MORB-type mantle field of 225 Ma ago (Fig. 8), the zircon syenite pegmatites and the hornblendite dyke show Sr–Nd isotopic signatures characteristic of the sources of ocean island basalts (OIB). Their intermediate position within the "mantle array" is representative of a less depleted mantle and may be interpreted as a mixture of depleted and enriched mantle, relative to bulk Earth. However, a distinct influence of the enriched mantle components EM I and/or EM II is not distinguishable from figure 8 (see also chapter 5.6).

## 5.6. PB ISOTOPIC COMPOSITION OF THE ZIRCON SYENITE PEGMATITES AND OF A HORNBLENDE SYENITE

$^{206}Pb/^{204}Pb$, $^{207}Pb/^{204}Pb$ and $^{208}Pb/^{204}Pb$ ratios were measured in feldspars from a zircon syenite pegmatite and from a hornblende syenite (Tab. 7). Due to very low U/Pb ratios in feldspar, the age corrections for the initial isotope ratios are minor. Therefore, the measured isotopic ratios of the feldspars from the Triassic dykes were used as initial ratios and are shown in figure 9.

*Tab. 6* Sr and Nd isotopic composition of a hornblendite dyke, apatite and calcite. In addition, the last two columns contain the isotopic data of the zircon syenite pegmatites (STÄHLE et al., 1990). Values for the Rb/Sr and $^{87}Sr/^{86}Sr$ ratios of bulk Earth used are 0.0816 and 0.7047, respectively.

| | hornblendite (wr) C550 | hornblendite (wr) C551 | calcite C550 | calcite C551 | apatite C550 | zircon syenite pegmatite S 8 | zircon syenite pegmatite S 9 |
|---|---|---|---|---|---|---|---|
| $^{87}Rb/^{86}Sr$ | 0.04208 | 0.00875 | 0.00060 | 0.00016 | 0.00031 | 0.000891 | 0.0001934 |
| $^{87}Sr/^{86}Sr$ | 0.703857(20) | 0.703700(20) | 0.703693(19) | 0.703681(21) | 0.703641 | 0.70459(4) | 0.70389(4) |
| $(^{87}Sr/^{86}Sr)_i$ | 0.703722 | 0.703672 | 0.703691 | 0.70368 | 0.70364 | 0.7037 | 0.7037 |
| $^{147}Sm/^{144}Nd$ | 0.1121 | 0.10984 | 0.10657 | 0.10572 | 0.10286 | 0.1027 | 0.0493 |
| $^{143}Nd/^{144}Nd$ | 0.512760(13) | 0.512745(11) | 0.512760(8) | 0.512734(11) | 0.512741(12) | 0.512793(16) | 0.512680(25) |
| $(^{143}Nd/^{144}Nd)_i$ | 0.512595 | 0.512583 | 0.512603 | 0.512578 | 0.51259 | 0.512642 | 0.522608 |
| $\varepsilon^0_{Sr}$ | –11.96 | –14.19 | –14.29 | –14.46 | –15.03 | –1.56 | –11.49 |
| $\varepsilon^{225}_{Sr}$ | –10.18 | –10.87 | –10.62 | –10.76 | –11.34 | –10.49 | –10.49 |
| $\varepsilon^0_{Nd}$ | 2.38 | 2.09 | 2.38 | 1.87 | 2.01 | 3.027 | 0.824 |
| $\varepsilon^{225}_{Nd}$ | 4.81 | 4.58 | 4.97 | 4.48 | 4.72 | 5.73 | 5.07 |

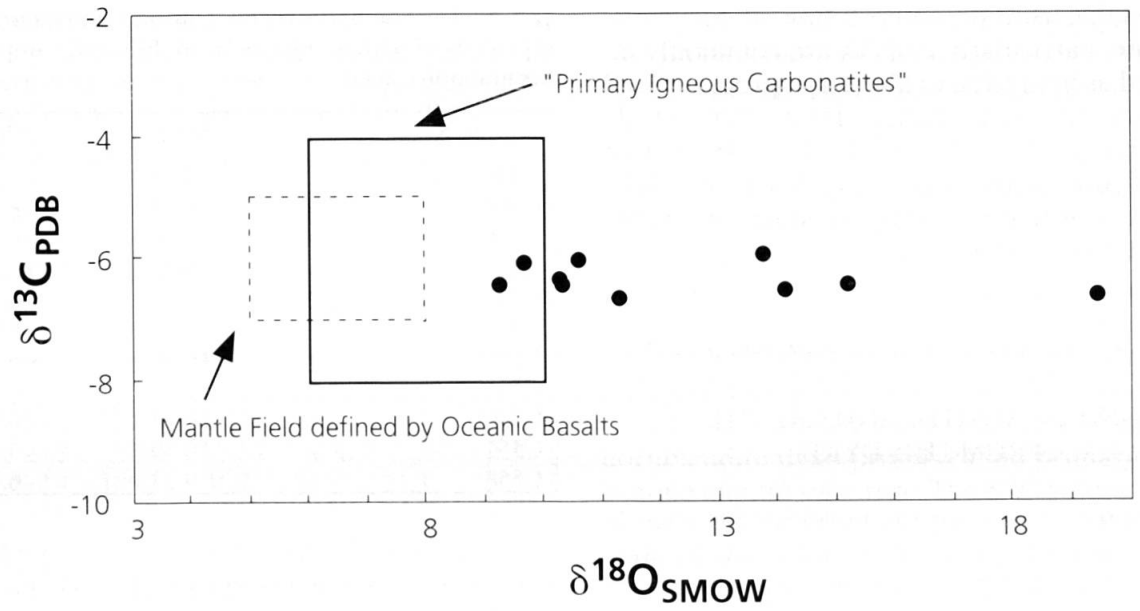


*Fig. 7* Stable isotopic composition $\delta^{13}C$ and $\delta^{18}O$ of matrix calcite from different samples of the hornblendite dyke (Tab. 5). The field of "primary igneous carbonatites" and the mantle field defined by oceanic basalts are taken from KELLER and HOEFS (1995).

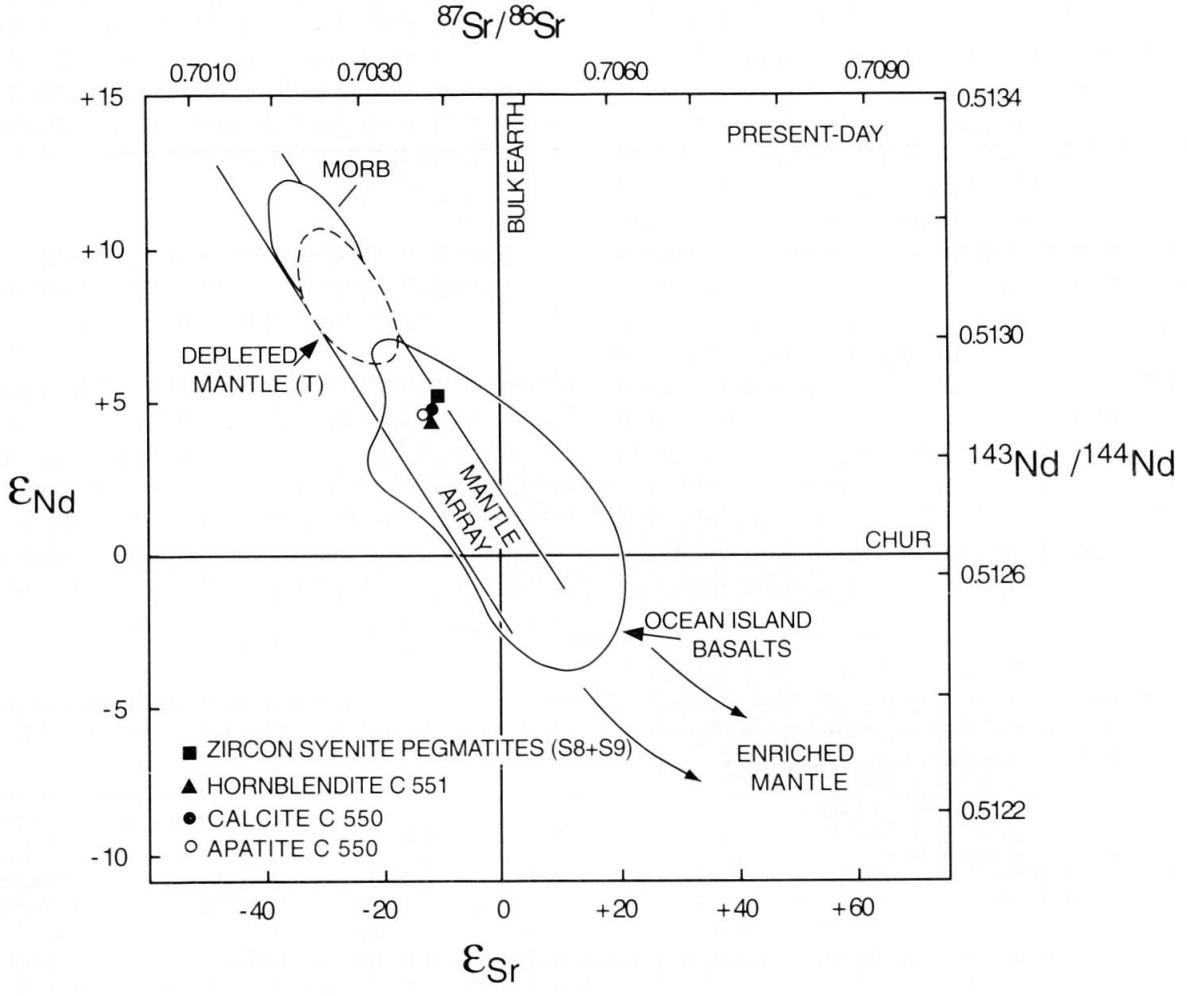


*Fig. 8* Present-day Nd and Sr isotopic variations of depleted and enriched mantle sources. Fields for mid-ocean ridge basalt (MORB) and oceanic island basalt (OIB) are shown (STÄHLE et al., 1990). Initial Sr and Nd isotopic ratios of the MORB-type depleted mantle (T) calculated for 225 Ma. Data symbol denote a zircon syenite pegmatite and a hornblendite dyke, together with apatite and calcite from the latter.

*Tab. 7* Pb isotopic composition of feldspars in a zircon syenite pegmatite (53/1,53/2) and of a hornblende syenite (C377).

| | $^{206}Pb/^{204}Pb$ | $^{207}Pb/^{204}Pb$ | $^{208}Pb/^{204}Pb$ |
|---|---|---|---|
| zircon syenite pegmatite 53/1 (feldspar) | 18.683 ± 0.011 | 15.577 ± 0.014 | 38.308 ± 0.047 |
| zircon syenite pegmatite 53/2 (feldspar) | 18.757 ± 0.014 | 15.589 ± 0.014 | 38.389 ± 0.048 |
| hornblende syenite C377 (feldspar) | 19.182 ± 0.023 | 15.618 ± 0.021 | 38.837 ± 0.062 |

*Tab. 8* K–Ar and $^{40}Ar/^{39}Ar$ results from various hornblende separates of a hornblende syenite and a hornblendite dyke (Fig. 10).

| Sample | Rock | Mineral fraction [µm] | Technique | K [%] | $^{40}Ar^*$ [nl/g] | Total Ar age [Ma] | Isochron age [Ma] |
|---|---|---|---|---|---|---|---|
| C535b | hornblendite | 200–315 | K–Ar | 1.210 | 21.79 ± 0.24 | 416.0 ± 5.4 | – |
| C535b | hornblendite | 200–315 | $^{40}Ar/^{39}Ar$ | – | – | 502.3 ± 2.4 | 276 ± 6 |
| C550 | hornblendite | > 200 | $^{40}Ar/^{39}Ar$ | – | – | 221.2 ± 1.6 | 206 ± 3 |
| C554b | hbl syenite | 200–315 | K–Ar | 1.335 | 12.47 ± 0.23 | 225.6 ± 4.5 | – |
| C554b | hbl syenite | 315–500 | K–Ar | 1.345 | 12.88 ± 0.07 | 230.9 ± 2.4 | – |
| C554b | hbl syenite | 315–500 | $^{40}Ar/^{39}Ar$ | – | – | 235.9 ± 1.7 | 223 ± 2 |

$^{40}Ar^*$ radiogenic argon; errors: internal 1 σ

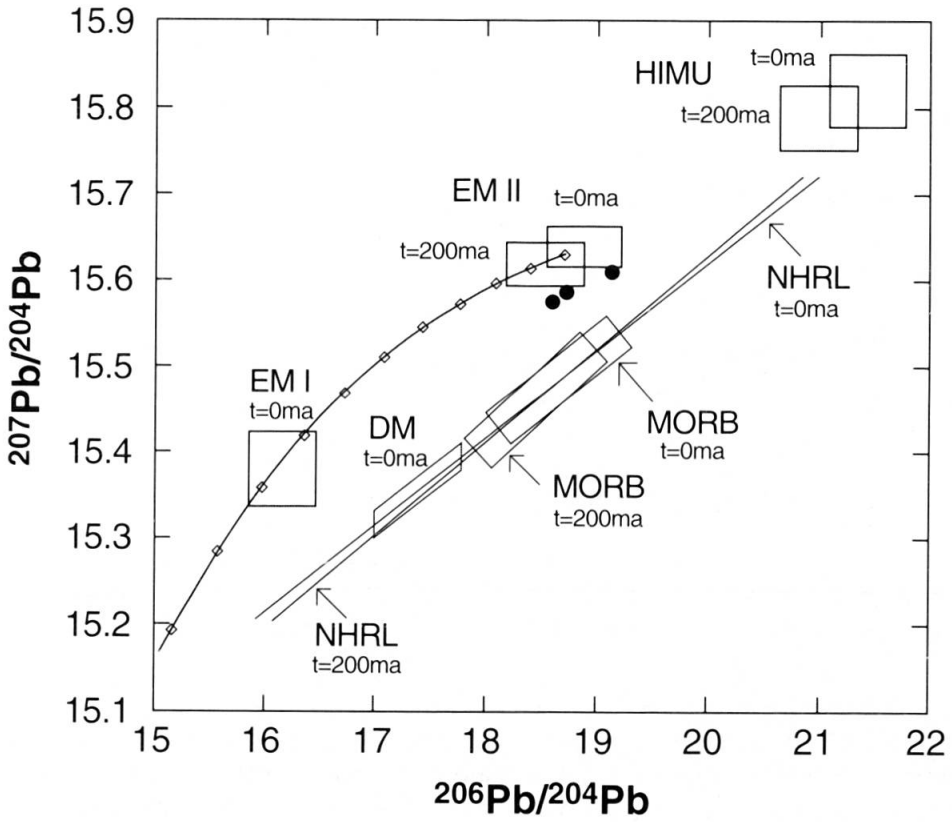


*Fig. 9* $^{207}Pb/^{204}Pb$ versus $^{206}Pb/^{204}Pb$ isotope variation diagram with the Northern Hemisphere Reference Line (NHRL). Data of the proposed mantle components and of some oceanic basalts are taken from ZINDLER and HART (1986): DM (depleted MORB mantle), HIMU (high U/Pb), EM I and EM II (enriched mantle).
Pb isotope compositions of a zircon syenite pegmatite (samples 53/1and 53/2) from Rio Creves and a hornblende syenite (sample C377) from Val Fiorina (Swiss Topographic map 285 Domodossola: kilometric grid 100.10/675.85) are shown.

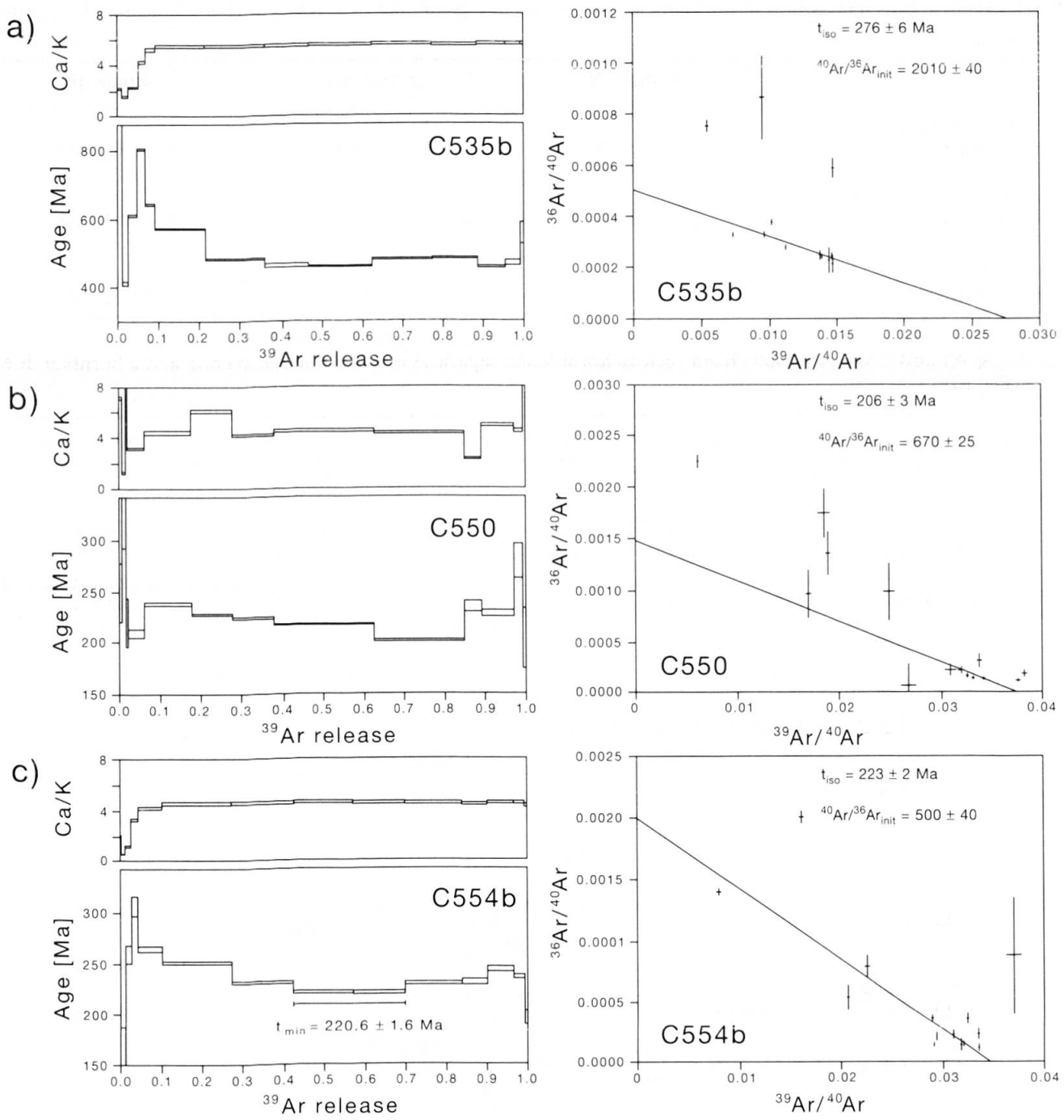


*Fig. 10* Ca/K spectra, step heating $^{40}Ar/^{39}Ar$ age spectra and isochron diagrams from various hornblende separates of a hornblende syenite and a hornblendite dyke. The rather constant Ca/K ratios of hornblende in the step heating experiments indicate high purity of the sample material, especially for C554b and C535.

The $^{207}Pb/^{204}Pb$ vs $^{206}Pb/^{204}Pb$ isotope diagram shows that the zircon syenite pegmatite (53/1, 53/2) and a hornblende syenite (C377) are enriched in radiogenic Pb (Fig. 9). The analyses lie above the Northern Hemisphere Regression Line (NHRL) and in proximity to the EM II reservoir, indicating slight depletion. Also shown in the diagram are the isotopic shifts of the various reservoirs since 200 Ma.

When interpreting the Pb isotope diagram, one may conclude that the source of the syenitic dyke rocks represents a mixture of the two endmembers DM and HIMU (ZINDLER and HART, 1986). A small contribution from the EM II reservoir is not unequivocally indicated in the diagram (Fig. 9), as the $^{208}Pb/^{204}Pb$ ratios of the syenitic rocks are relatively low as well (Tab. 7).

### 5.7. K–AR AND $^{40}AR/^{39}AR$ AGE DATA ON HORNBLENDE FROM SYENITE AND HORNBLENDITE DYKE ROCKS

Hornblende separates from a hornblendite and a syenite dyke yielded conventional K–Ar ages and integrated $^{40}Ar/^{39}Ar$ ages (Tab. 8) of 416 and 502 Ma (hornblendite C535b), 221 Ma (hornblendite C550) and 221 to 236 Ma (syenite C554b). Saddle-shaped age spectra and high $^{40}Ar/^{36}Ar$ initial ratios in the corresponding isochron diagrams (Fig. 10), indicate variable but high amounts of $^{40}Ar$ excess in all samples – a rather common finding on hornblende from the Alps. From the Finero area, hornblende with unusually high contents of $^{40}Ar$ has been previously reported by HUNZIKER (1974).

In the isochron diagram, sample C535b yielded a $^{40}Ar/^{36}Ar$ initial ratio of $2010 \pm 40$ and an isochron age of $276 \pm 6$ Ma (Fig. 10a; calculated from all data points). The broad scatter in the three isotope correlation diagrams indicates an inhomogeneous isotopic composition of the incorporated initial Ar, hence it is not possible to ascribe any geological significance to the obtained isochron age.

The total Ar age of 221 Ma obtained on sample C550 (Tab. 8) agrees with the single zircon evaporation age of $225 \pm 13$ Ma of a zircon syenite pegmatite which had been interpreted as the age of emplacement of the felsic dykes (STÄHLE et al., 1990). Similar age values in the range between 227 and 215 Ma were obtained by Sm–Nd dating on garnetiferous gabbroic rocks (LU et al., 1992). However, the irregularly shaped Ca/K distribution pattern of sample C550 (Fig. 10b) derived from the $^{37}Ar/^{39}Ar$ release ratios hints at a polyphase composition of this hornblende. Measurement effects such as $^{39}Ar$ redistribution during neutron-irradiation and irregular Ar degassing behaviour during vacuum release may influence the Ar isotope ratios of the sample resulting in artificially disturbed age and isochron diagrams. In such a case, interpretation of the isotope data concerning $^{40}Ar$ loss or excess is difficult, and the apparent ages obtained as well as the calculated $^{40}Ar/^{36}Ar$ initial ratio must be taken with some reservation. Thus, from the results on hornblende C550 no further geological conclusions should be drawn.

The saddle-shaped age spectrum of hornblende sample C554b exhibits a minimum age of 221 Ma (Fig. 10c) which can be interpreted as the maximum age of the geological process to be dated. Isochron calculation (all release steps) yielded an identical age of 223 Ma and an increased $^{40}Ar/^{36}Ar$ initial ratio of $500 \pm 40$. Because of the $^{40}Ar$ excess problem it is reasonable to avoid an over-interpretation of the latter age data. Nevertheless, they are not inconsistant with the intrusion of the syenite dyke between 225 and 220 Ma ago which is at present the most plausible interpretation of the age results on C554b hornblende.

## 6. Discussion

### 6.1. THE PERMIAN MAFIC FORMATION

(1) *Lower Permian magmatism.* The Lower Permian magmatism in the Southern-Alpine domain belongs to the post-Variscan era. The widespread magmatic intrusions into the consolidated European fold belt and into large parts of its northern foreland are associated with deep reaching dextral and divergent wrench faults between Gondwana and Laurussia forming pathways for the basaltic liquids which were produced in large masses within the upper mantle. Tensional stresses due to crustal shortening of the Appalachian-Mauretanides Fold belt were responsible for the development of this penetrative dextral fracture system in the European Variscides (ZIEGLER, 1993a).

The MORB-like tholeiitic magma of the Mafic Formation shows a strongly fractionated pattern (Fig. 4). In contrast to the uncontaminated rocks in the Finero area (LU et al., 1997b), most of the metagabbroic rocks in the Sesia valley assimilated crustal material (VOSHAGE et al., 1990, SINIGOI et al., 1994). However, in both areas the magmatic rocks of the Mafic Formation lost their original compositional signature of the primary magma.

(2) *Magmatic underplating.* Primary, dense melts from the mantle will tend to underplate the base of the continental crust. Ponding magmas must fractionate and assimilate crust-derived melts in order to surmount the density contrast and to reach the surface as evolved liquids. A model for the evolved basaltic liquids and their concealed cumulates along the Moho is given by COX (1980).

Magmatic underplating of the lower crust (VOSHAGE et al., 1990; SINIGOI et al., 1994), the interpretation of the voluminous, fractionated metabasalts as flood basalts (STÄHLE, 1991), and the widespread Permian calc-alkaline magmatism (e.g. BONIN et al., 1993), topped by rhyolitic volcanism in the Southern Alps, are in accordance with magmatic sequences found in many flood basalt provinces (VEEVERS, 1989).

(3) *The geophysical Ivrea body.* The Mafic Formation as a lower crustal intrusion transects the

whole Ivrea zone and occupies approximately 50% of its present outcrop area (Fig. 2). Tholeiitic flood basalts usually have equivalent portions of dense cumulates at depth (COX, 1980). Therefore, a dense cumulate body must exist beneath the surface of the Ivrea zone.

The flaky structure of the Western Alps is well constrained by geophysical cross sections (ROURE et al., 1990; MARCHANT and STAMPFLI, 1997). In the ECORS-CROP seismic geotraverse (NICOLAS et al., 1990) the Apulian Moho was found at a deeper level. The Ivrea Bouguer anomaly requires a larger volume of Apulian lower crust in the Ivrea body than previously thought (REY et al., 1990). In a deep tectonic model along transverse cross sections of the Western Alps, THOUVENOT (1984) also showed that the anomalous steep mantle wedge of the geophysical Ivrea body has a slightly lower density of $\rho = 3.22$ g/cm$^3$ than the "autochthonous" upper mantle with $\rho = 3.28$ g/cm$^3$.

According to the pronounced gravity high along the Ivrea-Verbano zone (BAYER et al., 1989) the presence of a dense olivine/pyroxene cumulate at depth could be an alternative to the proposed models. This idea is supported by the fractionated pattern of the metabasalts with their low mg#-values and their distinct Ni and Cr-depletion as demonstrated in the spidergram (Fig. 4). As an alternative view, the geophysical Ivrea body could be a composite dense crustal wedge composed of lower crustal felsic garnet granulites with large portions of an ultramafic residue from which the metabasalts on the surface were extracted as evolved tholeiitic melts.

### 6.2. THE TRIASSIC ALKALINE DYKE ROCKS

(1) *Metasomatic enrichment and lithospheric depth of the dykes.* Metasomatic processes in the

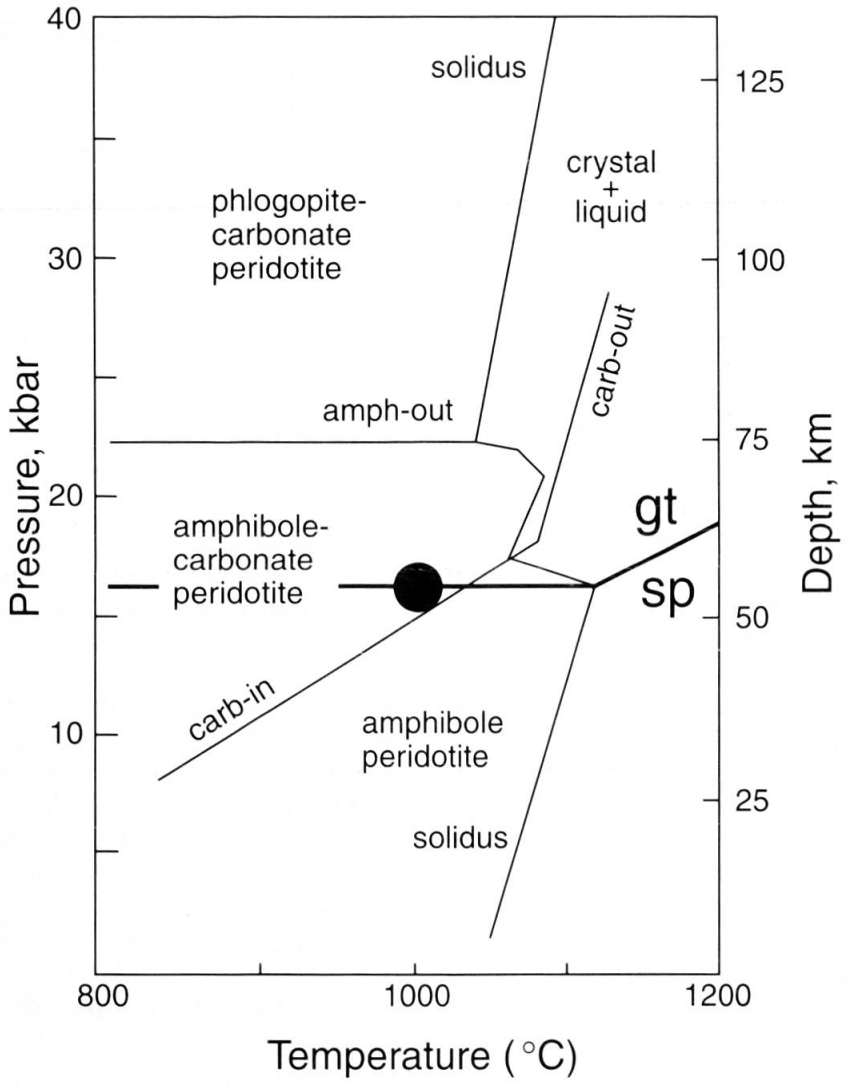


*Fig. 11* Stability relations of carbonated and hydrated peridotite are from figure 6.1b in WATSON et al. (1990). The black point in the graph represents the hypothetical magma source of the hornblendite dyke within the lithospheric subcontinental mantle.

Finero peridotite are documented by the occurrence of about 1–5 vol% of uniformly dispersed hornblende and phlogopite in the updomed ultramafic body. A 297 Ma metasomatic event contaminated the Finero protolith (VOSHAGE et al., 1987), and the high Sr-isotopic composition of the contaminating fluids indicate that this occurrence is not related to the Triassic alkali-magmatic dyke intrusions.

The dyke rocks within the strongly depleted Finero peridotite are low-volume partial melts originating from a metasomatically enriched upper mantle source. Contrary to kimberlites with steep chondrite-normalised REE-patterns, the incompatible element-enriched zircon syenite pegmatites have REE contents with low $(La/Yb)_{cn}$ ratios in the range of 14–15 (STÄHLE et al., 1990), indicative of a relatively shallow, subcontinental mantle source.

Taking into consideration the mineral composition of the hornblendite dyke, the stability relationships of hydrated and carbonated peridotite allows an exact characterization of the lithospheric magma source. The ultramafic dyke is alkaline with Na > K. Calcite in the matrix of the dyke shows a kinked slope in its chondrite-normalized REE patterns (Fig. 6). This indicates melting within a garnet-free or garnet-deficient mantle source. On the other hand, the stability field of calcite in the upper mantle is limited at lower pressures. Based on the phase diagram of figure 11 (WATSON et al., 1990), the melting zone of the hornblende dyke must lie in the transition zone of garnet and spinel peridotite at a depth of 45–55 km, equivalent to prevailing pressures of 15–18 kbar. Partial melting of the lihospheric source of the dykes must have started at temperatures of about 970–1030 °C.

(2) *Isotope and trace elements.* Sr and Nd isotopes indicate that the alkaline dyke rocks in the Finero peridotite have isotopic composition of ocean island basalts (OIB). Their ultimate source is "asthenospheric" deriving from a moderately depleted upper mantle source (Fig. 8). Quite similar isotopic ratios, with high Sm/Nd and low Rb/Sr ratios relative to bulk Earth, characterize Mesozoic doleritic dykes from Liberia and the Horingbaai dolerites from southern Africa (DUPUY et al., 1988; DUNCAN et al., 1990). Both were classified as asthenospheric derivatives intruded at early stages during the breakup of Pangea.

(3) *Intraplate magmatism: "plume" origin versus lithospheric extension.* Continental magmas can arise in active continental margins and in intraplate environments either through lithospheric extension along deep reaching shear zones or through plumes (TURCOTTE and OXBURGH, 1973). Magma formation in a convergent margin is excluded for the Triassic dykes because of the high Ta(Nb) contents of the zircon syenite pegmatites. A rift environment in the northern Ivrea zone is poorly defined (STÄHLE et al., 1990). However, compressional features in the Southern Alps during the Triassic period are well known from field observations (DOGLIONI, 1987; CASTELLARIN et al., 1988) and the EW-striking hornblende syenite dyke of figure 4 shows ± NS-directed pressures at a late crystallization stage.

OIB-like minor or trace element patterns in some continental magmas alone are insufficient to discriminate a mantle plume from an asthenospheric upper mantle source rising passively due to lithospheric extension and thinning (HAWKESWORTH and GALLAGHER, 1993). Whether extension-related magmatism or a plume impact at the bottom of the lithosphere is responsible for the observed magmas may be determined by means of further geological observations on rocks deposited on the surface.

The Ivrea zone is deeply eroded and bare of any sedimentary cover, but sedimentary Triassic rocks are found in the eastern parts of the Southern Alps on the "labile shelf" (BECHSTÄDT et al., 1978) where ingressions and regressions of the Tethys sea have been documented by a thick pile of Mesozoic sedimentary marine and terrestrial rocks (BOSELLINI, 1998). There, the sedimentary stratum should document all of the volcanic fall deposits and any motion of the continental crust.

(4) *Age relationship of Triassic magmatic and terrigenous sediments in the Southern Alps.* A distinct mid-Triassic thermal event is well documented in the whole area of the Southern Alps (FERRARA and INNOCENTI, 1974; BERTOTTI and TER VOORDE, 1994; LU et al., 1997b). In the Orobic section of this area (around Lake Como in figure 1) anatectic pegmatites were emplaced into the middle crust and the post-kinematic textures of the country rocks suggest that no pervasive deformation took place during the heating event (SANDERS et al., 1996).

Volcanic rocks exist as Middle Triassic tuffs and tuffite layers in the Lugano area (HELLMANN and LIPPOLT, 1981) and tuffaceous greenish "pietra verde" horizons occur within the marine Ladinian limestone in the area of the Dolomites (Fig. 1). The plutonic rocks of the 230 Ma old Monzoni intrusive complex (Fig. 1) are alkaline and characterized by K-rich "shoshonitic" chemical affinity. However, all the observed magmatic features in the Southern Alps belong to the same Middle Triassic thermal event.

Above the Lower Triassic Skythian Werfener formation in the area of the Dolomites, three conglomerate layers occur within the Anisian marine limestones, which may be explained by synsedimentary tectonics and/or sea-level fluctuations. However, the terrigenous top, an Upper Anisian Richthofen conglomerate horizon, is remarkable as no abrasional hinterland could be found (HEISSEL, 1982), and the regional flow directions of the coarse pebble deposits are radially arranged (ZÜHLKE, 1996). Between the uplifted zones, which are covered by the Upper Anisian Richthofen conglomerate, and the beginning of the Ladinian volcanics, which are embedded in the subsiding marine "Buchensteiner" limestones, a distinct time delay of at least 3–5 Ma exists.

(5) *Plate tectonics and geodynamic model.* From the "OIB"-type asthenospheric signature of the mid-Triassic dykes and the lack of wide extensional movements in the Southern-Alpine crust at that time, we conclude that an "active" asthenospheric upwelling triggered the magmatism.

A mantle plume will leave five different fingerprints on the lithosphere and overlying crust: push from below and uplift on top; erosion of the base of the lithosphere; input of heat; intrusion of melts and fluids; and eventually a hot-spot track on the surface. The asthenospheric melts may metasomatize advectively the shallow mantle lithosphere (see figures 20.17 and 20.19 in WYLLIE, 1989; BAILEY, 1987) while conductive heating of the lower lithosphere (TURNER et al., 1996) causes nearly contemporaneous steepening of the geotherms with second-stage melting of the metasomatic layers (RYABCHIKOV, 1995).

A hot-spot track with a time-related succession of the Triassic magmatics is not seen it the Southern Alps, although the "OIB"-type signature of the alkaline dykes would be in accordance with a "plume" upwelling.

Compared to normal basalts, alkaline rocks are produced by lower degrees of partial melting. From recycling of oceanic lithosphere and delamination of orogenic lithosphere in the Proterozoic and Phanerozoic, a lot of "OIB" source material may reside as dispersed streaks within the convecting upper mantle (ALLÈGRE and TURCOTTE, 1986; WILSON, 1993). At low degrees of partial melting the enriched scattered material in the asthenosphere would melt first and its geochemical characteristics would dominate the depleted MORB source reservoir (WILSON, 1993). Under these conditions the alkaline dykes should be interpreted as derivatives from the convecting asthensphere instead of originating from a deeper "plume" upwelling.

The ultimate driving force of plate tectonics is the loss of heat from the convecting upper mantle, whereas plumes appear to be driven by heat loss from the core (HILL et al., 1992).

During the Permo-Triassic the continents were assembled in the super-continent Pangea. This mega-continent covered about 30% of the terrestrial surface and was surrounded by the Panthalassa ocean. The insulating effect of the giant landmass provoked a distinct heat anomaly (ANDERSON, 1982) with a density-driven asthenospheric return flow underneath (BISCHOFF, 1985; PAVONI, 1985)) and a complete reorganization of the global upper mantle convection system (ZIEGLER, 1993b). At about the Middle/Late Triassic boundary (230 ± 5 Ma) the onset of continental rifting heralded the dispersal of Pangea (VEEVERS, 1989).

During the Permo-Triassic the Ivrea zone is placed in an area at the eastern margin of Pangea. In the Upper Triassic a distinct 20–30 Ma long thermal peak within the crust (SANDERS et al., 1996), along with uplift in some places and magma intrusions preceding cooling, normal faulting and extension in the area of the Southern Alps, give strong evidence of an "active" asthenospheric mantle upward flow. In contrast, the model of "passive" rifting postulates that extension should come first.

## 7. Conclusions

The Lower Permian metabasalts of the Ivrea zone are classified as anorogenic magmas developed in a transtensional rift setting (HANDY and ZINGG, 1991). It is very likely that the voluminous basaltic melts originated within the subcontinental mantle where they were formed passively by lithospheric extension (MENZIES and BODINIER, 1993). Geodynamically, this strong magmatism, which is not restricted to the Southern Alpine domain, belongs to the Europe-wide post-Variscan magmatic activity during the Lower Permian.

The fractionated tholeiitic basalts of the Mafic Formation leave voluminous olivine/clinopyroxene cumulates at the crust-mantle boundary. This dense cumulate layer together with garnetiferous lower crustal rocks in the present high crustal position is first and foremost responsible for the positive gravity anomaly in the Western Alps, and very likely corresponds to the modeled geophysical Ivrea body.

At the beginning of the Upper Triassic, alkaline dyke intrusions into the northern Ivrea zone originated at a depth of around 50 km. They were formed by second-stage melting of a metasomati-

cally enriched upper mantle, but their ultimate source was "asthenospheric". The time delay between the uplift of the crust, documented by the Upper Anisian Richthofen conglomerate in South Tyrol, and the somewhat younger Ladinian/Carnian magmatism in the Southern-Alpine domain is a striking fact. This is explained by the impingement of a "hot" new upwelling asthenosphere at the base of the lithosphere and the long duration of the conductive heat transfer into the overlying mantle, later triggering melting of volatile-rich material.

Likewise, the upwelling branch of the convecting asthenosphere gave birth to the larger Monzoni intrusive complex in the eastern part of the Southern Alps at the Ladinian (Fig. 1). The "shoshonitic" chemical composition of the Mt. Monzoni magmatic rocks is probably controlled by older metasomes from the Hercynian orogenic cycle (CRISCI et al., 1984; BONADIMAN et al., 1994) pre-existing within the lithospheric mantle. Thus, with the "new" upwelling of the convecting asthenosphere, the actual start of the "Alpine cycle" may be in the Anisian.

**Acknowledgements**

We are grateful to R. Altherr for his friendly assistance and critical remarks. The long-standing support of H.J. Lippolt is particularly well received. A. Baumann, W. Hansmann, V. Köppel and B. Kober gave invaluable assistance in isotope analyses and interpretation. Thanks to Z. Berner, V. Garasic, S. Hoernes, H.-W. Hubberten, M. Koch, H.P. Meyer, H. Puchelt, N. Scheele, O. Werner and D.W. Zachmann for much help and assistance in the laboratory and finally to P. Polich for assistance with the manuscript. In the end, the manuscript profited on a bigger scale from two anonymous reviewers.

**References**

ALLÈGRE, C.J., PINEAU, F., BERNAT, M. and JAVOY, M. (1971): Evidence for the occurrence of carbonatites on the Cape Verde and Canary Islands. Nature Phys. Sci. 233, 103–104.

ALLÈGRE, C.J. and TURCOTTE, D.L. (1986): Implications of a two-component marble-cake mantle. Nature 323, 123–127.

ANDERSON, D.L. (1982): Hotspots, polar wander, Mesozoic convection and the geoid. Nature 297, 391–393.

BAILEY, D.K. (1987): Mantle metasomatism – perspective and prospect. In: FITTON, J.G. and UPTON, B.G.J. (eds): Alkaline igneous rocks. Geol. Soc. Spec. Publ. 30, Blackwell, Oxford, 1–13.

BARBOZA, S.A., BERGANTZ, G.W. and BROWN, M. (1999): Regional granulite facies metamorphism in the Ivrea zone: Is the Mafic Complex the smoking gun or a red herring? Geology 27, 447–450.

BAYER, R., CAROZZO, M.T., LANZA, R., MILETTO, M. and REY, D. (1989): Gravity modelling along the ECORS-CROP vertical seismic reflection profile through the Western Alps. Tectonophysics 162, 203–218.

BECHSTÄDT, Th., BRANDNER, R., MOSTLER, H. and SCHMIDT, K. (1978): Aborted rifting in the Triassic of the Eastern and Southern Alps. N. Jb. Geol. Paläont. Abh. 156, 157–178.

BERCKHEMER, H. (1969): Direct evidence for the composition of the lower crust and the Moho. Tectonophysics 8, 97–105.

BERTOTTI, G. and TER VOORDE, M. (1994): Thermal effects of normal faulting during rifted basin formation, 2. The Lugano-Val Grande normal fault and the role of pre-existing thermal anomalies. Tectonophysics 240, 145–157.

BISCHOFF, G. (1985): Die tektonische Evolution der Erde von Pangäa zur Gegenwart – ein plattentektonisches Modell. Geol. Rundsch. 74/2, 237–249.

BONADIMAN, C., COLTORTI, M. and SIENA, F. (1994): Petrogenesis and T–$fO_2$ estimates of Mt. Monzoni complex (Central Dolomites, Southern Alps): a Triassic shoshonitic intrusion in a transcurrent geodynamic setting. Eur. J. Mineral. 6, 943– 966.

BONIN, B., BRÄNDLEIN, P., BUSSY, F., DESMONS, J., EGGENBERGER, U., FINGER, F., GRAF, K., MARRO, Ch., MERCOLLI, I., OBERHÄNSLI, R., PLOQUIN, A., von QUADT, A., VON RAUMER, J., SCHALTEGGER, U., STEYRER, H.P., VISONA, D. and VIVIER, G. (1993): Late Variscan magmatic evolution of the Alpine basement. In: VON RAUMER, J.F. and NEUBAUER, F. (eds): Pre-Mesozoic geology in the Alps. Springer-Verlag, Berlin, 171–201.

BORIANI, A.C. and VILLA, I.M. (1997): Geochronology of regional metamorphism in the Ivrea-Verbano Zone and Serie dei Laghi, Italian Alps. Schweiz. Mineral. Petrogr. Mitt. 77, 381–401.

BORSI, S., FERRARA, G., PAGANELLI, L. and SIMBOLI, G. (1968): Isotopic age measurements of the M. Monzoni intrusive complex. Miner. Petrogr. Acta 14, 171–183.

BOSELLINI, A. (1998): Geologie der Dolomiten. Athesia-Verlag, Bozen. 192 S.

CASSINIS, G., MASSARI, F., NERI, C. and VENTURINI, C. (1988): The continental Permian in the Southern Alps (Italy). Z. geol. Wiss. Berlin 16, 1117–1126.

CASTELLARIN, A., LUCCHINI, F., ROSSI, P.L., SELLI, L. and SIMBOLI, G. (1988): The Middle Triassic magmatic-tectonic arc development in the Southern Alps. Tectonophysics 146, 79–89.

COX, K.G. (1980): A model for flood basalt volcanism. J. Petrol. 21, 629–650.

CRISCI, C.M., FERRARA, G., MAZZUOLI, R. and ROSSI, P.M. (1984): Geochemical and geochronological data on Triassic volcanism of the Southern Alps of Lombardy (Italy): genetic implications. Geol. Rundsch. 73/1, 279–292.

CULLERS, R.L. and GRAF, J.L. (1984): Rare earth elements in igneous rocks of the continental crust: predominantly basic and ultrabasic rocks. In: HENDERSON, P. (ed.): Rare earth element geochemistry. Elsevier, Amsterdam, 237–274.

DAL PIAZ, G.V. (1993): Evolution of Austro-Alpine and upper Penninic basement in the northwestern Alps from Variscan convergence to post-Variscan extension. In: VON RAUMER, J.F. and NEUBAUER, F. (eds): Pre-Mesozoic geology in the Alps. Springer-Verlag, Berlin, 327–344.

DAL PIAZ, G.V. and MARTIN, S. (1998): Evoluzione litosferica e magmatismo nel dominio Austro-Sudalpino dall'orogenesi Varisica al rifting Mesozoico. Mem. Soc. Geol. It. 53, 43–62.

DALTON, J.A. and WOOD, B.J. (1993): The compositions of primary carbonate melts and their evolution through wallrock reaction in the mantle. Earth Planet. Sci. Lett. 119, 511–525.

DOGLIONI, C. (1987): Tectonics of the Dolomites (Southern Alps, Northern Italy). J. Struct. Geol. 9, 181–193.

DUNCAN, A.R., ARMSTRONG, R.A., ERLANK, A.J., MARSH, J.S. and WATKINS, R.T. (1990): MORB-related dolerites associated with the final phases of Karoo flood basalt volcanism in southern Africa. In: PARKER, A.J., RICKWOOD, P.C. and TUCKER, D.H. (eds): Mafic dykes and emplacement mechanisms. Balkema, Rotterdam, 110–129.

DUPUY, C., MARSH, J., DOSTAL, J., MICHARD, A. and TESTA, S. (1988): Asthenospheric and lithospheric sources for Mesozoic dolerites from Liberia (Africa): trace element and isotopic evidence. Earth Planet. Sci. Lett. 87, 100–110.

ECORS-CROP DEEP SEISMIC SOUNDING GROUP (1989): Mapping the Moho of the Western Alps by wide-angle reflection seismics. Tectonophysics 162, 193–202.

FERRARA, G. and INNOCENTI, F. (1974): Radiometric age evidences of a Triassic thermal event in the Southern Alps. Geol. Rundsch. 63, 572–581.

FIORENTINI POTENZA, M., SCHWANDER, H. and STERN, W. (1975): Chemical distribution patterns in the Tertiary and Triassic igneous districts of the Central Alps. Chem. Erde 34, 257–282.

FOUNTAIN, D.M. and SALISBURY, M.H. (1981): Exposed cross-sections through the continental crust: implications for crustal structure, petrology, and evolution. Earth Planet. Sci. Lett. 56, 263–277.

FREY, F.A., GREEN, D.H. and ROY, S.D. (1978): Integrated models of basalt petrogenesis: a study of quartz tholeiites to olivine melilitites from south eastern Australia utilizing geochemical and experimental petrological data. J. Petrol. 19, 463–513.

FROITZHEIM, N., SCHMID, ST.M. and FREY, M. (1996): Mesozoic paleogeography and the timing of eclogite-facies metamorphism in the Alps: A working hypothesis. Eclogae geol. Helv. 89/1, 81–110.

GEBAUER, D. (1993): The pre-Alpine evolution of the continental crust of the Central Alps – an overview. In: VON RAUMER, J.F. and NEUBAUER, F. (eds): Pre-Mesozoic geology in the Alps. Springer-Verlag, Berlin, 93–117.

HANDY, M.R. and ZINGG, A. (1991): The tectonic and rheological evolution of an attenuated cross section of the continental crust: Ivrea crustal section, southern Alps, northwestern Italy and southern Switzerland. Geol. Soc. Am. Bull. 103, 236– 253.

HAWKESWORTH, C.J. and GALLAGHER, K. (1993): Mantle hotspots, plumes and regional tectonics as causes of intraplate magmatism. Terra Nova 5, 552–559.

HEISSEL, W. (1982): Südtiroler Dolomiten. Sammlung Geologischer Führer, Bd. 71, Gebrüder Borntträger-Verlag, Berlin. 172 S.

HELLMANN, K.N. and LIPPOLT, H.J. (1981): Calibration of the Middle Triassic time scale by conventional K–Ar and $^{40}Ar/^{39}Ar$ dating of alkali feldspars. J. Geophys. 50, 73–88.

HESS, J.C., LIPPOLT, H.J. and KOBER, B. (1995): The age of the Kagenfels granite (northern Vosges) and its bearing on the intrusion scheme of late Variscan granitoids. Geol. Rundsch. 84, 568–577.

HILL, R.I., CAMPBELL, I.H., DAVIES, G.F. and GRIFFITHS, R.W. (1992): Mantle plumes and continental tectonics. Science 256, 186–193.

HOFFBAUER, R. and SPIERING, B. (1994): Petrologic phase equilibria and stable isotope fractionations of carbonate-silicate parageneses from granulite-grade rocks of Sri Lanka. Precambrian Res. 66, 325–349.

HOGARTH, D.D. (1989): Pyrochlore, apatite and amphibole: distinctive minerals in carbonatite. In: BELL, K. (ed.): Carbonatites, genesis and evolution. Unwin Hyman, London, 105–148.

HUBBERTEN, H.W., KATZ-LEHNERT, K. and KELLER, J. (1988): Carbon and oxygen isotope investigations in carbonatites and related rocks from the Kaiserstuhl, Germany. Chem. Geol. 70, 257–274.

HUNZIKER, J.C. (1974): Rb–Sr and K–Ar age determination and the Alpine tectonic history of the Western Alps. Mem. Ist. Geol. Mineral. Univ. Padova 31, 1–54.

IRVINE, T.N. and BARAGAR, W.R.A. (1971): A guide to the chemical classification of the common volcanic rocks. Canad. J. Earth Sci. 8, 523–548.

KELLER, J. and HOEFS, J. (1995): Stable isotope characteristics of recent natrocarbonatites from Oldoinyo Lengai. In: BELL, K. and KELLER, J. (eds): Carbonatite volcanism. Springer-Verlag, Berlin, 113–123.

KOGARKO, L.N. , HENDERSON, C.M.B. and PACHECO, H. (1995): Primary Ca-rich carbonatite magma and carbonate-silicate-sulphide liquid immiscibility in the upper mantle. Contrib. Mineral. Petrol. 121, 267–274.

KÖPPEL, V., HANSMANN, W. and MAGGETTI, M. (1997): Pb isotope and trace element signatures of polymetamorphic rocks from the Silvretta nappe, a comparison. Schweiz. Mineral. Petrogr. Mitt. 77, 325–335.

LE BAS, M.J. (1984): Oceanic carbonatites. In: KORNPROBST, J. (ed.): Kimberlites, I: kimberlites and related rocks. Elsevier, Amsterdam, 169–178.

LE MAITRE, R.W. (1976): Some problems of the projection of chemical data into mineralogical classifications. Contrib. Mineral. Petrol. 56, 181–189.

LE MAITRE, R.W. (1989): A classification of igneous rocks and glossary of terms. Blackwell, Oxford. 193 pp.

LU, M., HOFMANN, A.W., RIVALENTI, G. and MAZZUCCHELLI, M. (1992): Geochemical and geochronological constraints on the origin of the mafic complex at Finero, Ivrea Zone. Europ. J. Mineral. 4, Bh. 1, 179.

LU, M., HOFMANN, A.W., MAZZUCCHELLI, M. and RIVALENTI, G. (1997a): The mafic- ultramafic complex near Finero (Ivrea-Verbano Zone), I. Chemistry of MORB-like magmas. Chem. Geol. 140, 207–222.

LU, M., HOFMANN, A.W., MAZZUCCHELLI, M. and RIVALENTI, G. (1997b): The mafic-ultramafic complex near Finero (Ivrea-Verbano Zone), II. Geochronology and isotope geochemistry. Chem. Geol. 140, 223–235.

MARCHANT, R.H. and STAMPFLI, G.M. (1997): Crustal and lithospheric structure of the Western Alps: geodynamic significance. In: PFIFFNER, O.A., LEHNER, P., HEITZMANN, P., MUELLER, ST. and STECK, A. (eds): Deep structure of the Swiss Alps: results of NRP 20. Birkhäuser-Verlag, Basel, 326–337.

MASCH, L. and HUCKENHOLZ, H.G. (1993): Der Intrusivkomplex von Monzoni und seine thermometamorphe Aureole. Eur. J. Mineral. 5, Bh. 2, 81–135.

MENZIES, M.A. and BODINIER, J.L. (1993): Growth of the European lithospheric mantle – dependence of upper-mantle peridotite facies and chemical heterogeneity on tectonics and age. Phys. Earth Planet. Int. 79, 219–240.

NICOLAS, A., POLINO, R., HIRN, A., NICOLICH, R. and ECORS-CROP working group (1990): ECORS-CROP traverse and deep structure of the western Alps: a synthesis. In: ROURE, F., HEITZMANN, P. and POLINO, R. (eds): Deep structure of the Alps. Mém. Soc. géol. France, N.S. 156, 15–27.

PAVONI, N. (1985): Die pazifisch-antipazifische Bipolarität im Strukturbild der Erde und ihre geodynamische Deutung. Geol. Rundsch. 74/2, 251–266.

PFIFFNER, O.A., LEHNER, P., HEITZMANN, P., MUELLER, ST. and STECK, A. (1997): Deep structure of the Swiss Alps: results of NRP 20. Birkhäuser-Verlag, Basel. 380 pp.

QUICK, J.E., SINIGOI, S. and MAYER, A. (1995): Emplacement of mantle peridotite in the lower continental crust, Ivrea-Verbano zone, northwest Italy. Geology 23, 739– 742.

REY, D., QUARTA, T., MOUGE, P., MILETTO, M., LANZA, R., GALDEANO, A., CARROZZO, M.T., BAYER, R. and ARMANDO, E. (1990): Gravity and aeromagnetic maps of the western Alps: contribution to the knowledge of the deep structures along the ECORS-CROP seismic profile. Mém. Soc. géol. France, N.S. 156, 107–121.

RICHARD, P., SHIMIZU, N. and ALLÈGRE, C.J. (1976): $^{143}Nd/^{146}Nd$, a natural tracer: an application to oceanic basalts. Earth Planet. Sci. Lett. 31, 269–278.

RIVALENTI, G., GARUTI, G., ROSSI, A., SIENA, F. and SINIGOI, S. (1980): Existence of different peridotite types and of a layered igneous complex in the Ivrea zone of the Western Alps. J. Petrol. 22, 127–153.

ROTTURA, A., DEL MORO, A., CAGGIANELLI, A., BARGOSSI, G.M. and GASPAROTTO, G. (1997): Petrogenesis of the Monte Croce granitoids in the context of Permian magmatism in the Southern Alps. Italy. Eur. J. Mineral. 9, 1293–1310.

ROURE, F., HEITZMANN, P. and POLINO, R. (1990): Deep structure of the Alps. Mém. Soc. géol. France, N.S. 156, 367 pp.

RYABCHIKOV, I.D. (1995): Different sources of kimberlites and carbonatite parent magmas: evidence from high pressure experiments and trace element geochemistry. Sixth International Kimberlite Conference, Novosibirsk, 706–707.

SANDERS, C.A.E., BERTOTTI, G., TOMMASINI, S., DAVIES, G.R. and WIJBRANS, J.R. (1996): Triassic pegmatites in the Mesozoic middle crust of the Southern Alps (Italy): Fluid inclusions, radiometric dating and tectonic implications. Eclogae geol. Helv. 89/1, 505–525.

SCHENK, V. (1981): Synchronous uplift of the lower crust of the Ivrea Zone and of Southern Calabria and its possible consequences for the Hercynian orogeny in Southern Europe. Earth Planet. Sci. Lett. 56, 305–320.

SCHMID, S.M., PFIFFNER, O.A., FROITZHEIM, N., SCHÖNBORN, G. and KISSLING, E. (1996): Geophysical-geological transect and tectonic evolution of the Swiss-Italian Alps. Tectonics 15, 1036–1064.

SINIGOI, S., QUICK, J.E., CLEMENS-KNOTT, D., MAYER, A., DEMARCHI, G., MAZZUCCHELLI, M., NEGRINI, L. and RIVALENTI, G. (1994): Chemical evolution of a large mafic intrusion in the lower crust, Ivrea-Verbano Zone, northern Italy. J. Geophys. Res. 99, 21575–21590.

STÄHLE, V. (1991): Die Ivrea-Zone: Petrochemische Untersuchungen an Karbonatiten, Zirkonsyeniten und Metabasalten. Habilitationsschrift, Geowissenschaftliche Fakultät, Universität Heidelberg.

STÄHLE, V., FRENZEL, G., KOBER, B., MICHARD, A., PUCHELT, H. and SCHNEIDER, W. (1990): Zircon syenite pegmatites in the Finero peridotite (Ivrea zone): evidence for a syenite from a mantle source. Earth Planet. Sci. Lett. 101, 196 – 205.

STÄHLE, V., FRENZEL, G., HESS, J.C., KÖPPEL, V., SAUPÉ, F. und SCHNEIDER, W. (1996): Die geotektonische Stellung des Magmatismus in der Ivrea Zone (Südalpen). Europ. J. Mineral. 8, Bh. 1, 274.

STAMPFLI, G.M. (1996): The Intra-Alpine terrain: A Paleotethyan remnant in the Alpine Variscides. Eclogae geol. Helv. 89/1, 13–42.

STEIGER, R.H. and JÄGER, E. (1977): Subcommission on geochronology: convention on the use of decay constants in geo- and cosmochronology. Earth Planet. Sci. Lett 36, 359–362.

THOUVENOT, F. (1984): Deep crustal structure of the Western Alps: present knowledge and pending problems. Mem. Soc. Geol. It. 29, 15–24.

TURCOTTE, D.L. and OXBURGH, E.R. (1973): Mid-plate tectonics. Nature 244, 337– 339.

TURNER, S., HAWKESWORTH, C., GALLAGHER, K., STEWART, K., PEATE, D. and MANTOVANI, M. (1996): Mantle plumes, flood basalts, and thermal models for melt generation beneath continents: Assessment of a conductive heating model and application to the Paraná. J. Geophys. Res. 101, 11503–11518.

VAI, G.B. and COCOZZA, T. (1986): Tentative schematic zonation of the Hercynian chain in Italy. Bull. Soc. géol. France 8, tome II, 95–114.

VEEVERS, J.J. (1989): Middle/Late Triassic (230 ± 5 Ma) singularity in the stratigraphic and magmatic history of the Pangean heat anomaly. Geology 17, 784–787.

VOSHAGE, H., HUNZIKER, J.C., HOFMANN, A.W. and ZINGG, A. (1987): A Nd and Sr isotopic study of the Ivrea zone, Southern Alps, N-Italy. Contrib. Mineral. Petrol. 97, 31–42.

VOSHAGE, H., HOFMANN, A.W., MAZZUCCHELLI, M., RIVALENTI, G., SINIGOI, S., RACZEK, I. and DEMARCHI, G. (1990): Isotopic evidence from the Ivrea Zone for a hybrid lower crust formed by magmatic underplating. Nature 347, 731–736.

WASS, S.Y., HENDERSON, P. and ELLIOTT, C.J. (1980): Chemical heterogeneity and metasomatism in the upper mantle – evidence from rare earth and other elements in apatite-rich xenoliths in basaltic rocks from eastern Australia. Phil. Trans. R. Soc. Lond., A297, 333–346.

WATSON, E.B., BRENAN, J.M. and BAKER, D.R. (1990): Distribution of fluids in the continental mantle. In: MENZIES, M.A. (ed.): Continental mantle. Clarendon Press, Oxford, 111–125.

WILSON, M. (1993): Geochemical signatures of oceanic and continental basalts: a key to mantle dynamics? J. Geol. Soc. Lond. 150, 977–990.

WOPFNER, H. (1984): Permian deposits of the Southern Alps as product of initial alpidic taphrogenesis. Geol. Rundsch., 73, 259–277.

WYLLIE, P.J. (1989): Origin of carbonatites: evidence from phase equilibrium studies. In: BELL, K. (ed.): Carbonatites – genesis and evolution. Unwin Hyman, London, 500–545.

ZIEGLER, P.A. (1993a): Late Palaeozoic–Early Mesozoic plate reorganization: evolution and demise of the Variscan fold belt. In: VON RAUMER, J.F. and NEUBAUER, F. (eds): Pre-Mesozoic geology in the Alps. Springer-Verlag, Berlin, 203–216.

ZIEGLER, P.A. (1993b): Plate-moving mechanisms: their relative importance. J. Geol. Soc. Lond. 150, 927–940.

ZINDLER, A. and HART, S. (1986): Chemical geodynamics. Ann. Rev. Earth Planet. Sci. 14, 493–571.

ZÜHLKE, R. (1996): Fazies, hochauflösende Sequenzstratigraphie und Beckenentwicklung im Anis (mittlere Trias) der Dolomiten (Südalpin, Italien). Dissertation, Naturwiss.-Math. Fakultät., Universität Heidelberg.

Manuscript received December 12, 1999; revision accepted November 11, 2000.